RSC Advances

REVIEW

View Article Online
View Journal | View Issue

Cite this: *RSC Adv.*, 2026, **16**, 2303

Color tuning in lanthanide ions doped upconversion nanocrystals

JiaYue Zhang,[a] Xinyu Wang,[a] Yuxin Jin,[a] Boyang Li,*[a] Lu Liu *[ab] and Jianzhong Zhang*[ab]

Received 17th October 2025
Accepted 15th December 2025

DOI: 10.1039/d5ra07944f

rsc.li/rsc-advances

Lanthanide ions doped upconversion nanocrystals, capable of changing their dominant emission bands and thus colors, have attracted increasing attention because of their abundant implementation ways, high feasibility, wide tuning range, and finally great application prospects. The unique 4f ladder-like arranged energy levels of lanthanide ions are the key towards their color tuning ability. In this review, we present a summary and discussion on the key aspects of the recent progress in Lanthanide-based color-tunable upconversion nanocrystals, *via* manipulations of intrinsic properties of nanocrystals as well as external experimental configurations. Benefitting from the multifunctional and versatile luminescence bands, the color-tunable upconversion nanocrystals exhibit great potential in diversities of cutting-edge applications such as display device, advanced anti-counterfeiting, optical coding, thermochromic-based thermometer, bioimaging, biosensing, and multifunctional phototherapy. The prospectives and challenges for the research in color-tunable upconversion nanocrystals are also provided. This review would be helpful in designing and building new lanthanide-based upconversion nanomaterials capable of manipulating more precisely the dominant emission bands and expand their application boundaries.

1. Introduction

The color of an object can change under different conditions, which is a common phenomenon in both natural and artificial materials and demonstrates high flexibility and broad adaptability in various application scenarios. Unlike the passive color-variable materials (*e.g.*, structural color and metachrosis) that are non-luminous, artificial self-emissive materials, especially nanomaterials, that emit switchable dominant light colors actively are highly promising in display,[1] sensing,[2] lighting,[3] exploration,[4] biomedicine,[5] and many other fields.

Among the active color-tuning mechanisms, photoluminescence is highly promising as a non-contact characterization and manipulation tool that directly probes and tune the intrinsic photophysical properties of materials. The photoluminescence-based color tuning uses excitation light to irradiate the luminescent objects and generate emission light with different wavelengths, which can be achieved intrinsically and externally: one can use different luminescent materials to emit different colors, *i.e.*, the multicolor tuning achieved by the change of intrinsic properties of materials.[6] These multicolor materials are needed for developing luminescent labels, especially for the multiplexed detection and multicolor imaging as they can distinguish different targets simultaneously after proper targeting modifications;[7] Alternatively, one can use an identical luminescent material to emit different colors by manipulation of the external conditions, namely, the real-time color tuning, which is particularly promising for full-color display and high-level security.[8]

Early color tuning efforts in luminescent nanomaterials were basically multicolor tuning, and mainly demonstrated in fluorescent dyes[9] and quantum dots (QDs).[10] Traditional fluorescent dyes have very bright emissions and abundant light colors, but still facing many difficulties such as photobleaching,[11] strong autofluorescence,[12] wide emission band,[13] short lifetime,[14] and small Stokes shift,[15] preventing them from the wide-range color tuning applications. From another side, QDs are also capable of wide-range emission that cover the full color gamut, and can overcome most of the problems for fluorescent dyes.[16] The biotoxicity, photo-blinking, and stability of the QDs, however, remain formidable challenges for the researchers. In addition, the carbon dots (CDs), first synthesized two decades ago, also exhibit fascinating properties as the multicolor nanomaterials.[17,18] However, the current synthesis techniques for preparing CDs involve complex purification steps and high consumption of organic solvents,[19] and the formation process and luminescence mechanism of CDs are not clear yet.[20–23] These limitations restrict the large-scale applications of CDs.

Alternatively, the inorganic lanthanide (Ln) upconversion nanocrystals (UCNCs) also serve as multicolor tuning

[a]*Key Lab of In-Fiber Integrated Optics of Ministry of Education of China, College of Physics and Optoelectronic Engineering, Harbin Engineering University, Harbin 150001, P.R. China. E-mail: liulu@hrbeu.edu.cn; zhangjianzhong@hrbeu.edu.cn; lby2565738163@163.com*

[b]*Key Laboratory of Photonic Materials and Devices Physics for Oceanic Applications, Ministry of Industry and Information Technology of China, College of Physics and Optoelectronic Engineering, Harbin Engineering University, Harbin 150001, China*

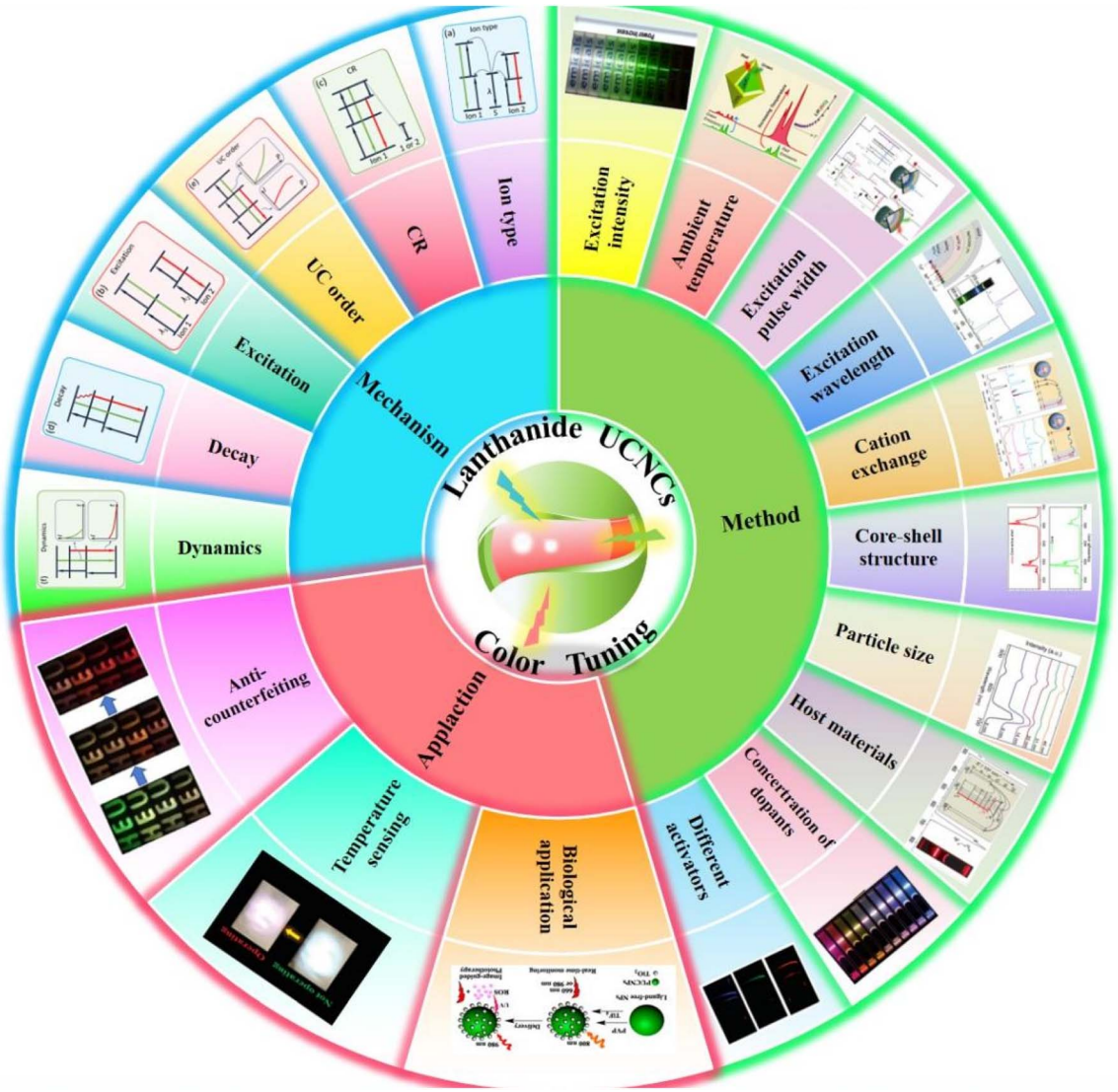

Fig. 1 Overview of Ln UCNCs color tuning, showing the main mechanisms, tuning strategies, and applications of the color-tunable UCNCs.

materials.[24–27] UC luminescence is a nonlinear anti-Stokes process, which requires two or more incident low-energy photons (mostly in NIR region) to induce one output high-energy photon (mostly in visible and UV region). Although holding much lower luminescent quantum yields (or efficiency), Ln UCNCs have many advantages over other multicolor nanomaterials, including low biotoxicity, excellent structural stability, nonblinking, rich emission colors, relatively narrow spectral bands, large anti-Stokes shift, long lifetimes, and facile construction of nanostructures.

Besides multicolor tuning, Ln UCNCs are especially suitable for real-time color tuning.[28] Among the above-mentioned advantages of Ln UCNCs, the abundant ladder-like arranged energy levels, facile core–shell (C–S) structures, and high-order anti-Stokes pathways are highly helpful to achieve the real-time color tuning. Specifically, although the emission peaks of Ln ions can be hardly changed due to the shield of outer electronic shells, the abundant energy levels and thus multiband emissions enable tuning relative emission intensity; the construction of C–S structure through epitaxial growth can not only significantly enhance the luminescent intensity but also combine different functions (like light colors) into one particle;[29] The anti-Stokes property, converting wavelength from NIR to Vis,[30] of UC luminescence avoids the interference of excitation light to the color observation, and provides more complex population pathways to increase the tuning feasibility.[31] Consequently, Ln doped UCNCs exhibit unique real-time color tuning ability, and have wide application prospects in the cutting-edge fields like information storage,[32] advanced anti-counterfeiting,[33] multi-wavelength lasing,[34] and laser-induced 3D display.[35]

In this review, we attempt to make a systematic summary and discussion on the key aspects, recent advances, and frontier applications of color-tunable UCNCs (Fig. 1). In Section 1, a brief introduction is presented to the color tuning phenomena, and the photoluminescence color tuning using Ln UCNCs was highlighted. In Section 2, we summarize the main properties of Ln UCNCs against other types of color-tunable

photoluminescence nanomaterials. Especially, the color tuning mechanisms are summarized. In Section 3, the specific strategies towards the UC color tuning are summarized first. Then, we attempt to provide a comprehensive survey of experimental results of UC color tuning, including the multicolor tuning and the real-time color tuning. In Section 4, after displaying a series of cutting-edge applications for the UC color tuning, challenges and prospects of the color-tunable UCNCs are presented. We believe this review will offer a thorough insight into the control of luminescence color of the UCNCs, which would help to explore new structural and spectral designs towards further wide-range, precise, and facile manipulation of the UC color and expand their application boundaries.

2. Overview of the ln UCNCs

The current photoluminescence-based color-tunable nanomaterials are mainly organic fluorescent nanoprobes, semiconductor and perovskite QDs, CDs, and Ln UCNCs. Among them, Ln UCNCs feature as many unique advantages and thus are more versatile as compared to others (Table 1). In this section, we will focus on the Ln UCNCs and discuss their main characteristics and luminescent mechanisms.

2.1 Main aspects of ln UCNCs

The Ln UCNCs, comprising active Ln ions and inert hosts, are mostly in the size range of ~10 nm–1 μm with various lattice structures and particle morphologies.[36–40] The Ln ions (mostly Ln^{3+} series) are only filled with electrons in the inner orbitals ($4f^{0-14}$) with the increase of atomic number, and the outer orbits (6s and 5d) are empty but still shield the inner ones. As a result, the luminescence of doped Ln^{3+} is similar to that of their free ions with narrow bands and is only slightly affected by the surrounding environment. More importantly, the abundant energy levels of Ln^{3+} enrich their emission colors, which also provide more opportunities for color-tuning by various ways, and make Ln UCNCs more versatile as compared to other color-tunable nanomaterials.

As for the Ln ions doped hosts, the early-stage hosts are mainly single crystals and glasses. Single crystal hosts provide strong local crystalline field but are difficult to synthesize, while glass hosts can be easily prepared and formed into flexible shapes, but with lower luminescence efficiency due to weak local crystalline field. In contrast, the NCs can be obtained through facile preparation and provide strong localized crystalline field, which has attracted increasing attention.

However, the nonradiative decay processes in the UCNCs are a large concern, due to the very large specific surface area of NCs brings strong energy trapping by the surface defects. Fortunately, this surface quenching effect can be greatly suppressed by some surface modification techniques like inert shell coating. From another side, low phonon-energy of the host is beneficial for the luminescence intensity. Ln UCNCs hosts include mainly halides, oxides, sulfide, *etc.* Among them, Ln ions doped fluorides like Er/Yb:$NaYF_4$ has become the most popular UCNCs, due to it makes a balance between luminescence performance and structural stability. On one hand, Er^{3+} and Yb^{3+} are the most efficient UC dopant pair; on the other hand, the $NaLnF_4$ host has relatively low phonon-energy (350 cm^{-1}), good physical and chemical stability, and highly controllable synthesis techniques like thermal decomposition[41] and hydrothermal method.[42]

Combining the Ln ions and the host materials, Ln UCNCs have exhibited many unique advantages, include but not limited to:

(i) The luminescence lifetime of Ln UCNCs ranges from around 10 μs to 20 ms, much longer than that of traditional dyes and QDs.

(ii) Their typical emission band width is several tens of nm, validates high throughput multiplexing applications.

(iii) The UC nature leads to very large anti-Stokes shift, effectively avoiding the possible spectral overlap between excitation and emission.

(iv) The high stability of the Ln^{3+} luminescence avoids the photo-blinking and bleaching.

(v) Low biotoxicity of the most-widely used $NaLnF_4$ NCs enable their *in vivo* applications.

(vi) The facile preparation of high-quality C–S NCs, and even core–multishell NCs, can improve the luminescent efficiency and combine different functions at one nanoparticle level.

These characteristics of Ln UCNCs can promote their wide applications such as display devices, anti-counterfeiting, photovoltaics, non-contact thermometers, bio-imaging, phototherapy, and so on.[43,44]

Table 1 Main aspects of widely-used color-tunable nanomaterials

Typical parameters	Organic dyes	QDs	CDs	Ln UCNCs
Materials	Cyanine and rhodamine	CdSe, InP, and $CsPbBr_3$	Carbon nucleus with functional groups	Er/Yb:$NaYF_4$, Tm,Yb:Y_2O_3, Nd:$CaWO_4$
Size	Below 1 nm	Below 10 nm	Below 10 nm	nm–μm
Shape	Molecules with multiple aromatic rings	Mostly spheres, a few rods and pyramids	Sphere-like	Spheres, rods, flakes, dumbbells, octahedrons
Mechanism	Stokes	Stokes	Stokes mainly	anti-Stokes
Excitation	Single band	Single band	Single band	Multiple bands
Lifetime	ns	ns–μs	ns	μs–ms
Stability	Poor stability	Poor stability	Stable	Stable
Toxicity	Dependent on dye materials	High risk from heavy metal	Low	Low
Tuning strategy	Multicolor	Multicolor	Multicolor	Multicolor, real-time tuning

2.2 Luminescence mechanisms of ln NCs

Compared to the traditional fluorescent materials, the UC luminescent mechanisms of Ln NCs are more complicated with many different mechanisms involved. As a result, the detailed mechanisms of UC luminescence are discussed in this section.[45] The luminescence of Ln^{3+} doped materials can be sorted as electroluminescence, photoluminescence, mechanoluminescence, thermoluminescence, *etc.* For the photoluminescence discussed in this review, it can be Stokes and anti-Stokes types, depending on the energy difference between incident and emitted photons.[46]

However, there are other terms describing the photoluminescence processes, like downconversion (DC), UC, quantum cutting (QC), and downshifting (DS), which somewhat arouse confusions. Among these terms, only UC is the anti-Stokes process in which two or more incident photons are absorbed and one high-energy photon is emitted, while DC, QC, and DS are all Stokes processes with higher photon energy absorbed than emitted. Though DC and DS are sometimes used to describe the same type of luminescence, conceptually, DC should be the reverse to UC. That means DC luminescence are the processes that materials absorb one high-energy incident photon and then emit two or more low-energy photons, which is the same as QC.[47,48] Finally, DS refers to particularly the Stokes luminescence that emit only one low-energy photon, with energy losses *via* mainly heat generation to satisfy the Energy Conservation Law.[49,50] The brief pathways for above-mentioned luminescence processes are depicted in Fig. 2.

Here, we will focus on the mechanisms of UC luminescence, comprising mainly three types of processes: excited-state absorption (ESA), energy transfer (ET), and photon avalanche (PA).

ESA mechanism was first proposed by Bloembergen in 1959, aiming at novel infrared detectors.[51] As depicted in Fig. 2, ESA usually occurs following the ground-state absorption (GSA). An ion in the excited-state absorbs a second photon before relaxing back to the ground-state and, as a result, goes to a higher energy level. Generally, the effective occurrence of ESA in Ln UCNCs requires two preconditions: one is the excited-state has a lifetime long enough to enable the secondary excitation; the other is the energy gap for ESA matches the excitation photon energy, or has a small mismatch considering the compensation from the host phonons. It is also possible to achieve multiple ESAs in Ln UCNCs, resulting in an even larger anti-Stokes shift. However, the UC luminescence is generally very weak due to the small absorption and excitation cross sections of Ln^{3+}.

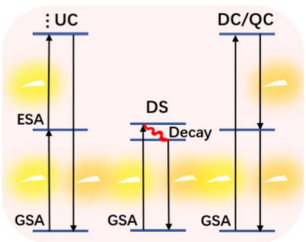

Fig. 2 Schematic diagrams of photoluminescence pathways of Ln ions.

As depicted in Fig. 3a and b, ET processes can be radiative (reabsorption of activator ion A from sensitizer ion S over a long propagation distance) and non-radiative (van der Waals-type Coulomb interaction between S and A).[52] The radiative ET usually lacks practical value due to its very low transfer efficiency, and therefore we focus on the non-radiative ET only. Non-radiative ET UC, first found in 1966,[53,54] is more effective as compared to the ESA UC. Once the S was doped into the UCNCs together with the A, owing to the much stronger light absorption of S associated with the highly efficient ET from S to A, the UC luminescence intensity can be greatly enhanced.

The most efficient non-radiative ET is known as the Förster resonant ET (FRET), which happens in S and A with well-matched energy gaps and between two different ($S \neq A$) or identical ($S = A$) ions. Especially, FRET that happens among the identical excited- and ground-states of same ions ($S = A$) is known as the energy migration (EM) process. While FRET between a high-energy state and a low-energy state, and then populates one identical intermediate state or two separated intermediate states, is the cross relaxation (CR) process. CR process can occur between two different ions ($S \neq A$) or two identical ions ($S = A$).

The occurrence of effective FRET requires the following preconditions: first, the large spectral overlap of S emission and A absorption. In another word, the well-matched energy gaps between S and A. Second, the shorten distance between S and A as the ET rate is reversely proportional to r^n (r is the distance, n = 6, 8, and 10 for dipole–dipole, dipole–quadrupole, and quadrupole–quadrupole interactions, respectively). This means the concentrations of S and A need to be elaborately chosen, ensuring strong interactions between them but in the meanwhile avoiding the concentration quenching effects. Third, the large emission cross section of S and large absorption cross section of A, as the ET rate is proportional to the product of these two parameters. Up to now, in UCNCs the Ln ions can serve as S are mainly Nd^{3+} at 800 nm, Yb^{3+} at 980 nm, and Er^{3+} at 1530 nm, while Ln ions suitable for A are Er^{3+}, Ho^{3+}, Tm^{3+}, *etc.*

In the case of small energy mismatch, non-radiative ET can be phonon-assisted, requiring lattice phonons involved to bridge the energy mismatch of S and A. Depending on the intervening manners of phonons, the phonon-assisted ET can be Stokes and anti-Stokes. The Stokes ET means S has a larger energy gap than A, so phonons are emitted to tailor the energy during the ET process. As for the anti-Stokes ET, the energy gap of S is smaller than that of A, and S requires absorbing phonons to compensate the energy difference. Clearly, the Stokes ET is an exothermic process, while the anti-Stokes ET is an endothermic process.

The third UC mechanism is PA, which is more complex and difficult to achieve due to PA is multi-step collaborations of ESA and CR, as depicted in Fig. 3c. In a typical PA dominant UC process, the excitation photon energy deviates the energy gap of GSA but matches that of the ESA. As a result, only small population at the intermediate state of Ln^{3+} can be found in the beginning. Although less population at intermediate state,

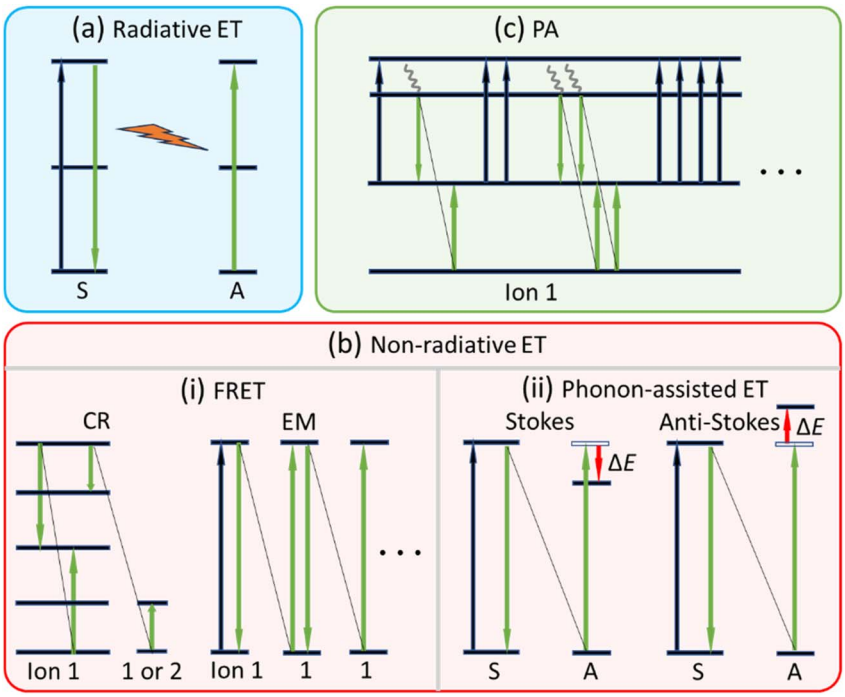

Fig. 3 Schematic diagrams illustrating the main ET pathways: (a) radiative ET, (b) non-radiative ET, and (c) PA.

there are still some ions can reach the high excited level *via* ESA. Focusing one ion in the high excited-state, the CR between this ion and another ion at the ground-state leads to two ions to be populated to the intermediate state. *Via* two ESA processes these two ions can jump to the high excited-state. Above-mentioned processes double the population of high excited-state and are cyclical till saturation, finally generate bright UC emissions. The PA UC requires a threshold laser intensity to initiate, and once the avalanche is built the UC response is highly nonlinear. This means an PA UC usually exhibits steep change in the power dependence variation. In addition, the PA requires a certain amount of irradiation time to begin, and then a longer time is required to achieve the maximum extent of the avalanche.[55] The key to achieve PA is a very weak GSA to ensure that only a small portion of ions are excited, and then a strong ESA activating the avalanche. The second prerequisite is the effective CR to maintain the avalanche. This requires a higher concentration of Ln^{3+} to provide sufficient neighboring ions for CR. However, it should be noted that excessive concentration of Ln^{3+} can cause concentration quenching, leading to the cessation of avalanche.

2.3 Color tuning mechanisms of ln UCNCs

Although the color tuning from Ln^{3+} UCNCs can be achieved *via* various strategies, the physical principle is quite simple. That is, changing the relative populations of different energy levels, whose emissions fall in the visible region. The possible mechanisms, which may not be fully realized yet, responsible for the UC color tuning comprise mainly the following types.

(i) Different colors from different Ln^{3+} using one excitation wavelength. The $4f^0$–$4f^{14}$ electronic configurations of Ln^{3+} enable various energy level arrangements, except the ions with empty (La^{3+})and full (Lu^{3+}) 4f orbits. Using UV light to excite the host materials or the high-energy states of Ln^{3+}, different Ln^{3+} can generate different emission colors, which were often found in the UV-activated DS phosphors.[56] This type of single-excitation-induced multicolor output is beneficial for specific applications like high-throughput multiplexing biolabeling. However, for ESA-based UC luminescence, using one excitation wavelength to generate different colors is difficult, due to the strict requirement of energy matching. Fortunately, the larger spectral overlap between S and A, as well as the Stokes or anti-Stokes assistance of phonons, make the ET UC easier to occur (like Yb^{3+}/Tm^{3+} and Yb^{3+}/Ho^{3+} codoped situations). Therefore, it is also possible to generate different colors from different Ln^{3+} *via* ET UC processes upon a single excitation source (Fig. 4a).

(ii) Different colors from different Ln^{3+} using multiple excitation wavelengths. The abundant and greatly varied energy levels of different Ln^{3+} enable different UC excitation pathways. It is therefore possible to find out at least two group of energy levels that validate the two independent UC emissions with different colors, upon different excitation wavelengths (Fig. 4b). Once such color tuning materials were found, one can use them separately towards the multicolor tuning. Alternatively, one can arrange different Ln^{3+} in different regions of one NC through construction of C–S structure, to achieve the real-time color tuning. Noted that for this real-time color tuning, the key is the independence of two UC emissions, otherwise different Ln^{3+} may all emit light simultaneously by any of the excitation wavelength. Another limitation of this strategy is the limited choices of excitation wavelength available for efficient UC luminescence.

(iii) Activating the CR process (Fig. 4c) or the nonradiative decay process (Fig. 4d) of same Ln^{3+} to emit different colors.

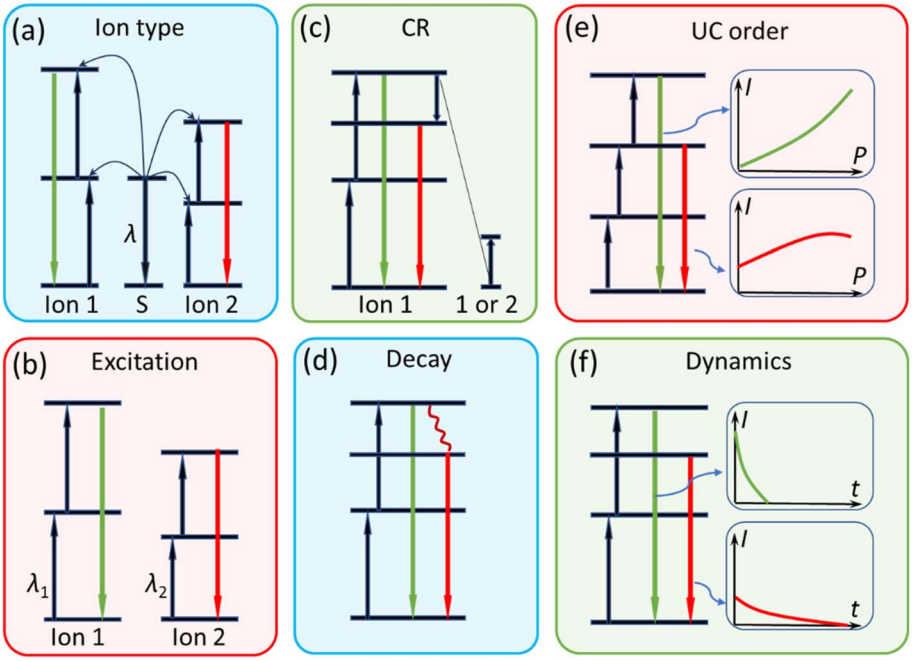

Fig. 4 Schematic diagrams illustrating the color change of Ln UCNCs based on different mechanisms.

These CR/decay processes usually related to two energy levels, which are accordingly responsible for different emission colors. During the CR/decay processes one state is depopulated, and meanwhile another state is fed. Additionally, these tuning processes can happen at the intermediate states, with the help of following ESA or ET UC pathway the emission color can also change. These CR processes can occur in same Ln^{3+} like Er^{3+} or between two different Ln^{3+} ions like Ho^{3+} and Ce^{3+}, Er^{3+} and Ce^{3+}, and Er^{3+} and Tm^{3+}.

(iv) Utilizing the different nonlinear orders of UC luminescence of Ln^{3+} (Fig. 4e). As discussed by Pollnau *et al.*, the UC intensity I is proportional to the n order of excitation intensity P, where n stands for the photon number involved in the UC process.[57] This well-known power dependence relation is valid when using weak excitation, indicating the decay dominates UC at the intermediate state. One can therefore draw the $\ln I$–$\ln P$ diagram and derive the slope from the obtained data, which is the UC order n. As shown in the insets of Fig. 4e, higher order UC luminescence generally requires higher excitation intensity to activate, but shows much brighter luminescence upon strong excitation as compared to the lower order UC luminescence. This means if two UC emission colors correspond accordingly to different UC orders, the lower-order UC color is dominant upon weak excitation, while higher-order UC color becomes overwhelming with increasing the excitation intensity. This strategy can be achieved in identical Ln^{3+} or different Ln^{3+}.

(v) Using dynamic excitation to generate the non-steady-state color change of UCNCs. The luminescence dynamics of different energy levels of Ln^{3+} are usually different, which enables the non-steady-state tuning of the emission color. As illustrated in Fig. 4f, one can choose UNNCs with, *e.g.*, strong intensity and rapid decay for one color and weak intensity and slow decay for another color, different color can be then observed in different time domains using the time-gating technique.[32] Like the decay dynamics, the rise (population) times of different Ln^{3+} energy states are also different. Therefore, one can combine the population and decay dynamics together, achieving more complex color change. For every excitation pulse, the fast color component would appear first and then the mixture of two colors, and then the mixture color gradually changes to slow color component till extinguishment. Similar to the above strategy, this strategy can be achieved also in identical Ln^{3+} or different Ln^{3+}.

2.4 Color tuning strategies of Ln UCNCs

There are numerous ways that can tune the emission color of Ln UCNCs, and they are basically *via* the manipulation of internal properties and/or external conditions of the UCNCs. The color tuning strategy, based on changing the internal (intrinsic and inherent) properties, relies primarily on the compositions of dopant and host. This means one material is used to generate one emission color, and different colors appear by changing the materials, forming the multicolor tuning phenomena. On the contrary, different colors are generated from a fixed composition without replacing the luminescent material, usually depend on the external surrounding conditions, leading to the real-time color tuning phenomena. Multicolor tuning can be achieved in both DS and UC luminescence, while real-time color tuning works are usually demonstrated in UCNCs. This is due to the more complicated pathways of UC luminescence provides more opportunities for manipulation of the dominant emission band.

For multicolor tunable UCNCs, their intrinsic properties are usually determined by the synthesis. The intrinsic properties of UCNCs that related to their luminescence colors include

mainly: (i) particle composition. Particle composition refers to the type and concentration of the dopants as well as the composition of the host materials. Different dopant ions usually emit different light colors, and even for the same dopant, the emission color is generally related to its doping concentration.[58] In addition, the host materials also influence the UC processes of Ln ions *via* different ways. (ii) Particle size and morphology. The extremely small size of NCs, *i.e.*, large specific surface area, amplifies the effects of the surface defects and ligands on the UC luminescence. Thus, the particle size and morphology usually alter the emission color, although might be not so evident as their effects on the luminescence intensity. (iii) Surface modification and coating. Besides altering the specific surface area, one can directly change the surface conditions of UCNCs *via* various surface modifications,[59–65] leading to the color change.

In real-time color-tunable UCNCs, their external conditions that affect the UC color are mainly excitation settings,[66] ambient temperature,[67] pH value,[68] humidity,[69] electromagnetic fields,[70,71] *etc.* Among these external conditions the excitation settings are more convenient and thus attracted most attention. These strategies mainly include: (i) switching excitation wavelength. The UC color of Ln ions can be evidently changed by using different excitation wavelengths, as incident photons with different energy may populate different states.[66] (ii) Tuning excitation intensity. The increase of the excitation intensity, *i.e.*, the excitation power density, will enhance the luminescence intensity. Noted that different emission bands of Ln ions usually have varied power-dependences, and thus show different UC color with the change of excitation intensity.[72] (iii) Altering excitation pulse width. Compared to the steady-state excitation situations, pulse excitations with different widths and waveforms provide new opportunities towards the UC color tuning, due to they can change the population pathways.[35]

Unlike the excitation settings, other external conditions like ambient temperature, pH value, humidity, and electromagnetic fields usually only alter the UC color slightly, due to the shield of outer electronic shells for the 4f–4f transitions. These surrounding conditions cause different effects, specifically, the phonon-assisted nonradiative relaxation is sensitive to the ambient temperature;[73] the pH value influences the fluorescence emission intensity of UCNCs in some medium;[74] the humidity related to the surface O–H ligands influence the surface quenching;[75] the electromagnetic field is positively correlated to the absorption and emission ability of Ln ions.[76] These effects aroused by external conditions all influence the population processes and thus change the UC color.

3. Results of color tuning in ln UCNCs

The past two decades have witnessed the great progress of Ln-based UCNCs from fundamental to applications. Especially, the color tuning using Ln UCNCs are particularly fascinating as it has shown promising potentials in many cutting-edge fields.[77,78] This Section will summarize and discuss the typical color tuning efforts. The typical color tuning results are summarized in Table 2, and will be discussed in detailed as follows.

3.1 Multicolor tuning in ln UCNCs

Multicolor tuning can easily reach full-color gamut by mixing the R/G/B UCNCs with proper ratios. Another advantage is their facile synthesis, as these multicolor NCs usually require only simple structures. Consequently, the luminescent properties of multicolor NCs are highly predictable, as the structure–performance relationships are well-established in the NCs with simple composition and structure.

Multicolor UCNCs are often adopted to display colored pattern by using different UCNCs together, distributed or overlapped. The main disadvantage of multicolor tuning is the limited flexibility and low spatial resolutions, as the light color from a fixed position is unchanged and different colors are separated spatially. Although the color tuning at a position can be achieved through changing the luminescent materials, it is highly inconvenient for applications that require timely color change.[88–90]

In the following subsections, we will summarize the main implementation strategies capable of manipulating the intrinsic properties of UCNCs that related to their luminescence colors.

3.1.1 Applying different activators. In previous Section 2.4, we briefly introduced the mechanisms of multicolor tuning *via* changing the type of Ln activator A. The core of this scheme lies in the fact that different A have different energy levels capable of emitting visible photons with different wavelengths, among their rich 4f configuration. The most popular A are Er^{3+}, Tm^{3+}, and Ho^{3+}, as they all have long-lived intermediate energy states to enable further upward populations, and large spacing energy levels resulting in weak nonradiative decays. The Er^{3+} and Ho^{3+} are mostly as the sources of green and red colors, while Tm^{3+} is the most-widely used blue UC light emitter.

Besides activators, sensitizers S are usually codoped into the multicolor UCNCs.[79,91–94] S are often used to pursue brighter UC luminescence, through strong energy harvest of S and then efficient ET from S to A. The traditional UC S is Yb^{3+} with only two energy levels within the 4f configuration, and their energy gap of $\sim 10^4$ cm^{-1} matches well with the commonly used A like Er^{3+}, Tm^{3+}, and Ho^{3+}. The UC mechanisms involving different codoped UCNCs are illustrated in Fig. 5a–c. For *in vivo* applications, the excitation of Yb^{3+} at around 980 nm overlaps with the absorption of water. Although this overlap exists, the absorption is moderate (approximately 10–100 m^{-1}) and the reduced tissue scattering still allow 980 nm to be widely used as a compromise wavelength for *in vivo* excitation. Nevertheless, to further enhance the excitation efficiency and avoid even minor interference from water absorption, Nd^{3+} sensitizers have been developed, because Nd^{3+} exhibits much stronger absorption at 800 nm, which falls in the highly transparent biological window. It is noteworthy that C–S or even complex core–multishell structures are usually required for Nd^{3+}-sensitized UCNCs, to maintain strong sensitization of Nd^{3+} and meanwhile avoid detrimental CR between A and Nd^{3+}. Recently, Er^{3+}-sensitized UCNCs[95] as well as Er^{3+} self-sensitized UCNCs,[96,97] excited by 1530–1550 nm photons, are proposed and attracted wide attention.

Table 2 Summary of the typical color tuning results

Composition (mol%)	Layer	Strategy	Shape	Sizes (nm)	E_x (nm)	Color (source)	Ref.
$NaYbF_4$:Tm $NaYbF_4$:Ho $NaYbF_4$:Er $NaYF_4$:Yb	1	Activators	Hexagonal plate	20	980	Blue (Tm^{3+}) Green (Ho^{3+}) Red (Er^{3+}) Pink (Yb^{3+})	79
$NaYF_4$:18Yb/2Er $NaYF_4$:20Yb/0.2Tm $NaYF_4$:25–60Yb/2Er $NaYF_4$:20Yb/0.2Tm/0.2–1.5Er	1	Dopants concentration	Hexagonal plate	N.A.	980	Green (Er^{3+}), blue (Tm^{3+}), red (Er^{3+}), gradually changed	58
$NaYF_4$:18–60Yb/0–1.5ErTm	1	Dopants concentration	Hexagonal plate	10–30	980	Green (Er^{3+}), blue (Tm^{3+}), red (Er^{3+})	7
$NaYF_4$:Yb/Er	1	Particle size	Hexagonal plate	6–45	980	Green (Er^{3+}), red (Er^{3+})	80
$NaYF_4$:5Yb/0.05Er @$NaYF_4$:20Yb/0.2Tm	2	Core–shell	Rod	~2000	980	Green (Er^{3+}), blue (Tm^{3+})	44
$NaYbF_4$:0–25Tb@$NaTbF_4$ $NaEuF_4$:0–25Tb@$NaTbF_4$	2	Cation exchange	Hexagonal plate	17	980	Green (Tb^{3+}), red (Eu^{3+})	81
$NaYF_4$:18Yb/2Er/40Mn @$NaYF_4$:10Yb @$NaNdF_4$:10Yb	3	Excitation wavelength	Dumbbell	25–60	808/980	Green (Er^{2+})/red (Mn^{2+})	77
$NaYF_4$:1Nd/30Yb/0.5Tm @$NaYF_4$:20Nd @$NaYF_4$ @$NaYbF_4$:25Er @$NaYF_4$	5	Excitation wavelength	Rod	49	808/980/1550	Blue (Tm^{3+})/red (Er^{3+})/green (Er^{3+})	78
$NaYbF_4$:0.1Tm/20Er @$NaYF_4$	2	Excitation wavelength	Hexagonal plate	130	980/1530	Red (Er^{3+})/green (Er^{3+})	82
$LiYbF_4$:1Tm @$LiGdF_4$ @$LiGdF_4$:18Yb/2Er @$LiYF_4$:40Nd/5Yb @$LiGdF_4$ @$LiErF_4$:0.3Tm @$LiGdF_4$	7	Excitation wavelength	Tetragonal bipyramidal	37	980/980/1550	Red (Tm^{3+})/blue (Tm^{3+})/green (Er^{3+})	29
$NaYF_4$:20Yb/1Tm @$NaYF_4$:20Yb/20Nd @$NaLuF_4$ @$NaYF_4$:20Yb/2Er @$NaLuF_4$ @$NaErF_4$:0.5Tm @$NaLuF_4$	7	Excitation wavelength	Sphere	83	808/808/1530	Green (Er^{3+})/blue (Tm^{3+})/red (Tm^{3+})	28
$NaGdF_4$:50Yb/1Tm @$NaGdF_4$:15Tb @$NaYF_4$:20Yb/2Er @$NaYbF_4$:50Nd @$NaYF_4$	5	Excitation wavelength	Hexagonal plate	65	808/980	Green (Er^{3+})/blue (Tm^{3+})	83
$NaGdF_4$:20Yb/2Er @$NaYF_4$ @$NaYF_4$:90Yb/2Tm @$NaYbF_4$:50Nd @$NaYF_4$	5	Excitation wavelength	Hexagonal plate	53	808/980	Green (Er^{3+})/blue (Tm^{3+})	84
$NaGdF_4$:Yb/Tm @$NaGdF_4$ @$NaYbF_4$:Nd @$Na(Yb,Gd)F_4$:Ho @$NaGdF_4$	5	Excitation wavelength	Rod	N.A.	808/976	Green (Ho^{3+})/blue (Tm^{3+})	85
Y_2O_3:10Yb/0.5Tm	1	Short pulse/long pulse	Sphere	16	980	Blue (Tm^{3+})/red (Tm^{3+})	6
$NaYF_4$:20Nd/20Yb @20Yb/0.2Tm @$NaYF_4$ @$NaYF_4$:20Yb/2Ho/8Ce @$NaYF_4$	5	Excitation wavelength/short pulse width/long pulse width	Hexagonal plate	~50	808/980	Blue (Tm^{3+})/green (Ho^{3+}) or red (Ho^{3+})	35

Table 2 (*Contd.*)

Composition (mol%)	Layer	Strategy	Shape	Sizes (nm)	E_x (nm)	Color (source)	Ref.
$LiErF_4$@$LiYF_4$	2	Low temperature/high temperature	Tetragonal bipyramidal	14–28	980	Green (Er^{3+})/red (Er^{3+})	86
$NaGdF_4$:18Yb/2Er @$NaGdF_4$ @$NaGdF_4$:Yb/Tm @$NaGdF_4$	4	Low to high excitation power density	Hexagonal rod	45	980	Green (Er^{3+}) to white (Er^{3+}, Tm^{3+})	87

The multicolor tuning by applying different activators typically demonstrates the R/G/B color components, because these R/G/B particles can be mixed to achieve the full color gamut, capable of showing any of the possible color component. A representative example for R/G/B multicolor tuning was demonstrated in 2008. Insets in Fig. 5a–c displayed the UC luminescence images of different A^{3+}-doped $NaYbF_4$ colloidal NCs under 980 nm excitation, which were taken without using any filters. The green emission from Ho^{3+}, red emission from Er^{3+}, and blue emission from Tm^{3+} could be distinguished by the naked eye.[79] Similarly, high purity of blue, green, and red UC emissions was achieved in Lu_2O_3:Yb/Tm, Lu_2O_3:Er, and Lu_2O_3:Yb/Er NCs, respectively.[98,99]

3.1.2 Adjusting the dopants concentration. As mentioned above, one can finely tune the emission color and obtain every color component within the full color gamut *via* mixing the R/G/B UCNCs. Another effective strategy towards the fine color tuning, and meanwhile avoiding the mechanical mixing, is adjusting the concentration of A and/or S. Specifically, the interactions between dopants, including CR between A, ET from S to A, backward ET from A to S, and EM among A or S, are different with the change of dopant concentration. These different interactions further influence the population pathways of A, resulting in varied relative intensities of different emission bands.

An impressive case that demonstrated fine-tuning of UC multicolor emissions by changing the dopant concentration was reported in 2008. $NaYF_4$ NCs containing a binary dopant (Er^{3+} and Yb^{3+}) exhibit an overall yellow light, comprising three sharp emission bands when excited at 980 nm, corresponding to the Er^{3+} blue transitions of $^2H_{9/2} \rightarrow {}^4I_{15/2}$, green transition of $^2H_{11/2}/{}^4S_{3/2} \rightarrow {}^4I_{15/2}$, and red transition of $^4F_{9/2} \rightarrow {}^4I_{15/2}$ (Fig. 6a).[58] The overall luminescent intensity of the three bands decreases gradually with increasing Yb concentration, due to enhanced backward ET from Er^{3+} to excess Yb^{3+}. Since the intensities of three emission bands vary differently with Yb^{3+} concentration, varied color output is achieved.

Noted that the blue emission is always much weaker than the green and red emissions, and thus the Er^{3+}-based multicolor tuning only exhibits green ↔ red change, even after carefully optimization. Therefore, Tm^{3+} is often adopted as the blue UC emitter ($^1D_2 \rightarrow {}^3F_4$ and $^1G_4 \rightarrow {}^3H_6$), exhibiting bright blue UC emission with excellent color purity, as demonstrated in the recent work.[100] Further, by introducing Tm^{3+} in the Yb^{3+}/Er^{3+} ternary system, the relative emission intensities originating from the two types of A^{3+} (Er^{3+} and Tm^{3+}) can be precisely

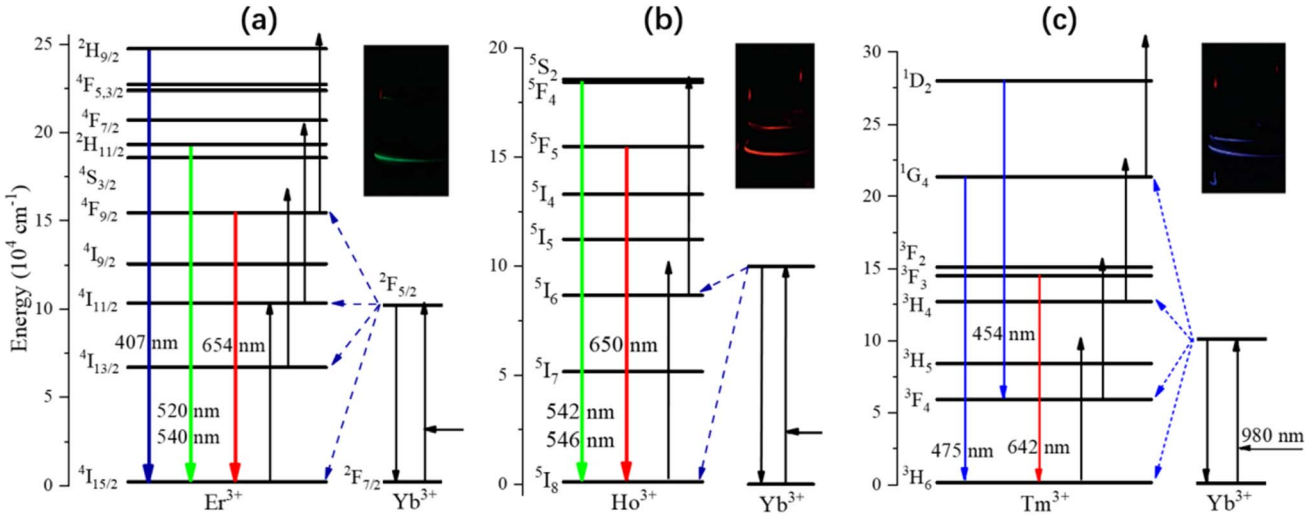

Fig. 5 Activator type-induced multicolor tuning in Ln UCNCs. UC pathways of Yb^{3+} sensitized (a) Er^{3+}, (b) Ho^{3+}, and (c) Tm^{3+} ions, only main ET from Yb^{3+} to activators as well as the visible luminescent transitions are labeled. Insets are the corresponding luminescent images of Er-, Ho-, and Tm-doped $NaYbF_4$ UCNCs prepared in chloroform solution, excited by 980 nm laser pointers. Reproduced with permission.[79] Copyright 2008, American Chemical Society.

controlled over a wider range. For example, Tm^{3+} is introduced in $NaYF_4$:Yb^{3+}/Er^{3+} NCs to add the blue color component, and further achieves fine-tuning of UC emission across the entire visible region (Fig. 6b).[58]

The main advantages of concentration-based multicolor tuning are its simplicity and feasibility. However, the disadvantage lies in its limited tuning performance, which usually allows for only moderate color change. Considering the most popular UC systems like Yb^{3+}/Er^{3+}, Yb^{3+}/Tm^{3+}, and Yb^{3+}/Ho^{3+} doped materials, multiple excited-states of activators can be populated, resulting multiple emission bands. It is difficult to avoid the appearance of other emissions while allowing a specific emission band.[101] Consequently, achieving high-color-purity (single-band) UC fluorescence remains a challenging task, especially for the red UC emission. Increasing the dopants concentration sometimes can achieve relatively pure red emission (Fig. 6a), but unfortunately, this strategy often quenches severely the overall luminescent intensity. Therefore, careful optimization of the dopant concentration is necessary to minimize the detrimental effects and meanwhile maintain high color purity and luminescent efficiency.

3.1.3 Assistance of the host materials. In addition to the dopants type and concentration, the host materials are also of vital importance for UC luminescent properties, as the Ln dopants are diffused into the host lattice and have strong interaction between dopant and host. The host can be single crystals, glasses, nano/microcrystals, glass ceramics, and organic molecules, showing different local crystallinity field effects, which lead to varied emission peak wavelength as well as band width, although quite slightly. Notably, much stronger effects of host materials on the UC properties are *via* the host absorption (creates excitons in conduction and valency bands), the ET between host and Ln, and the host phonon-related processes. Among them, the phonon-related processes are most common, which include multiphonon nonradiative decay and phonon-assisted ET. To pursue high luminescent brightness, low phonon-energy hosts capable of suppressing the multiphonon mediated energy dissipation are preferred. The effects of host materials on the luminescent color of Ln are also significant sometimes,[102] although most attentions are paid on the luminescent brightness. As mentioned above, one issue for multicolor NCs is the poor quality of red-light component. Noted that human eyes are more sensitive to green light. As a result, highly pure red light from Er^{3+} requires the red emission intensity is much stronger than that of the green band, forming the single-band red emission. To maintain both the high red color purity and the high luminescent intensity of Er^{3+} UC emission, utilizing UC processes assisted by host materials might be a promising solution.

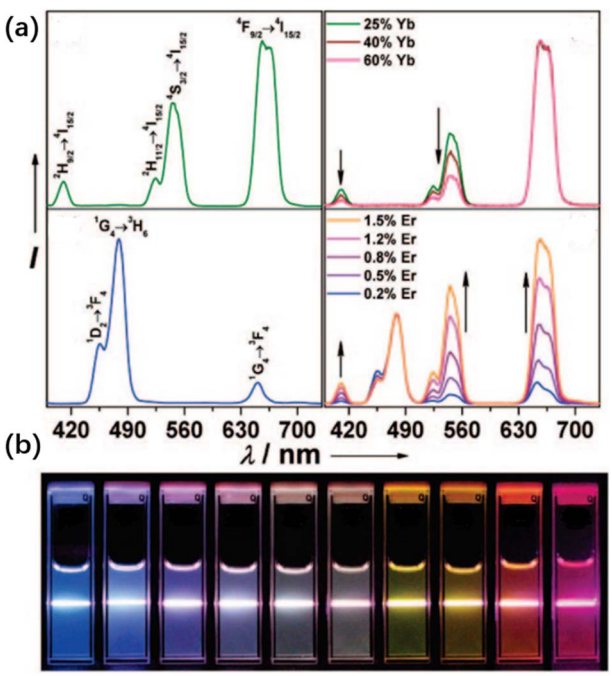

Fig. 6 Dopant concentration-induced multicolor tuning. (a) UC emission spectra of $NaYF_4$:Yb/Er (18/2 mol%), $NaYF_4$:Yb/Tm (20/0.2 mol%), $NaYF_4$:Yb/Er (25–60/2 mol%), and $NaYF_4$:Yb/Tm/Er (20/0.2/0.2–1.5) in ethanol solution (10 mM) at room temperature. Emission spectra of Er^{3+} and Tm^{3+} are normalized at 650 nm and 480 nm, respectively. (b) Luminescence images of the multicolor colloidal solutions, excited at 980 nm with a 600-mW diode laser. Reproduced with permission.[58] Copyright 2008, American Chemical Society.

Wang *et al.* proposed binary-doped (Yb/Er and Yb/Ho) $KMnF_3$ UCNCs that can generate high performance single-band red emission, under 980 nm irradiation (Fig. 7a).[102] This single-band UC emission can be attributed to the important role played by the host Mn^{2+} ions, *via* ET and backward ET processes. Taking $KMnF_3$: Yb/Er NCs for instance, the ET processes from $^2H_{9/2}$ and $^4S_{3/2}$ levels of Er^{3+} populate Mn^{2+} excited-state, which is slightly higher in energy than Er^{3+} red emitting level $^4F_{9/2}$. Followed by the backward ET from Mn^{2+}, Er^{3+} $^4F_{9/2}$ level is populated (Fig. 7a). These ET processes depopulate the high-energy blue and green levels and meanwhile feed the red energy level, thus enable the single-band red emission. The complete disappearance of blue and green emissions from Er^{3+} indicates highly efficient ET processes between Er^{3+} and Mn^{2+}. The situation in $KMnF_3$: Yb/Ho NCs is quite similar, also capable of single-band red emission originated from the $^5F_5 \rightarrow {}^5I_8$ transition (Fig. 7b). This strategy fills the gap of high-performance red UC emission and broadens the color tuning range.

Besides adopting Mn^{2+} in the host, researchers also tried to use other additives to achieve pure red emission with higher brightness, like adding Tm^{3+} ions for Er^{3+}-based materials and adding Ce^{3+} ions for Yb^{3+}/Ho^{3+} co-doped materials. These strategies can be classified as host-induced multicolor tuning, due to the additives (Tm^{3+} for Er^{3+} and Ce^{3+} for Ho^{3+}) occupy the host lattice site and serve as neither S nor A. Another typical case of multicolor tuning with the assistance of host materials was demonstrated in YVO_4,[7] although achieved by DS luminescence rather than UC luminescence. In contrast to the traditional $NaLnF_4$ materials, the host $[VO_4]^{3+}$ groups, with the help of Phosphorus ions, can generate strong blue emission. As the concentrations of A (Dy/Eu/Sm) increased, the emission of host material sacrifices and meanwhile is in favor of activator emission, exhibiting gradually changed emission color (Fig. 7c).

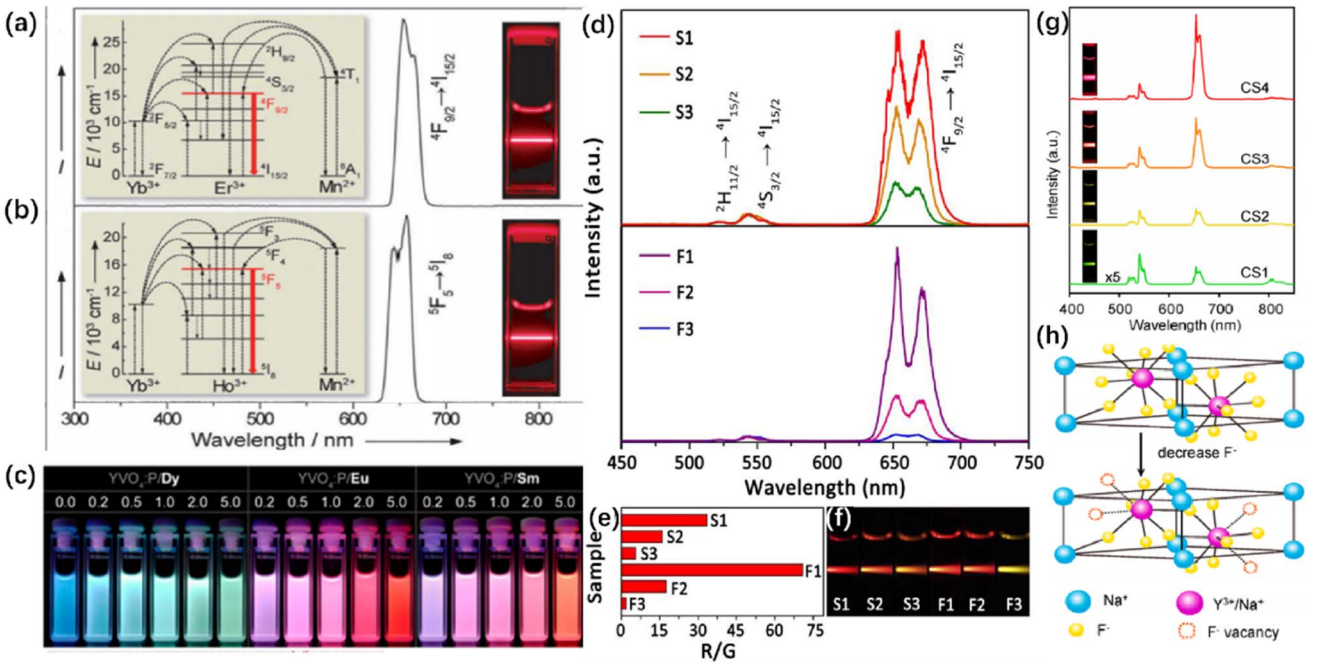

Fig. 7 Host-assisted multicolor tuning in Ln UCNCs. Room temperature UC emission spectra of (a) $KMnF_3$: Yb/Er (18 : 2 mol%) and (b) $KMnF_3$: Yb/Ho solution (18 : 2 mol%). Insets are the mechanisms responsible for the single-band red emission as well as the corresponding luminescent images, recorded under excitation from a 980 nm CW diode laser with a power density of 10 W cm^{-2}.[102] Copyright 2011, Wiley-VCH. (c) Luminescent images of YVO_4 NCs doped with phosphorus ions and different concentrations of Dy^{3+}, Eu^{3+}, and Sm^{3+}. Reproduced with permission.[7] Copyright 2014, American Chemical Society. (d) UC emission spectra of NCs upon 980 nm excitation with a power density of 10 W cm^{-2} (e) R/G ratios and (f) digital photographs of samples.[80] Copyright 2015, American Chemical Society. (g) UC emission spectra and corresponding luminescent photographs (insets) of the core–shell nanoparticles under 1540 nm laser excitation. (h) Schematic presentation of $NaErF_4$@$NaYF_4$ nanoparticles with decreasing F^- and inducing the atomic vacancies.[103] Copyright 2020, American Chemical Society.

Beyond the host–dopant interaction and phonon-related processes discussed above, the crystal structure of the host lattice plays a decisive role in governing lanthanide luminescence.[104] Lattice symmetry, site occupancy, and local coordination geometries determine the spatial distribution of dopants, the interionic distances, and the crystal-field splitting of 4f levels and the radiative transition rates. These structural factors in turn modulate the probabilities of resonant non-radiative ET and CR among neighboring Ln ions, and finally the emission colors. For example, phase-dependent local fields in $NaGdF_4$ (cubic *vs.* hexagonal) lead to markedly different ET dynamics. Hosts with multiple lanthanide sublattices or different-symmetry crystal fields often lead to preferential site occupation that changes emission branching ratios (Fig. 7d–f).[80] In addition, structural defects, cation vacancies, and non-stoichiometry can modify local crystal fields and lattice vibrations, thereby affect non-radiative decay pathways and alter UC emission profiles. Such host-structure-dependent effects have been experimentally demonstrated in several defect- and vacancy-engineered lanthanide nanomaterials (Fig. 7g and h).[103,105] These findings collectively highlight that controlling host structural parameters, including symmetry environment, lanthanide site occupation, and defect chemistry, is essential for tuning energy-migration networks and regulating both UC intensity and color.

3.1.4 Changing the particle size. Similar to the QDs, emission color of Ln UCNCs can also be changed by altering the particle size. The difference is that color tuning in QDs is governed by the quantum confinement effects, while Ln UCNCs often employ the significant quenching effect to tune their light colors by controlling the amount of surface defects at different sizes. The particle size of UCNCs can be manipulated by the precursors, reacting temperature and time,[106] solvents environment,[65] among others, during the synthesis.

Taking Er^{3+} and Yb^{3+} co-doped $NaYF_4$ NCs, again, as an example, the surface quenching becomes more prominent as the NCs size decreases from 45 nm to 6 nm.[107] As a result, the nonradiative decay process from $^4I_{11/2}$ to $^4I_{13/2}$ becomes stronger in smaller particles, the following ET from Yb^{3+} to Er^{3+} $^4I_{13/2}$ state dominates in ultra-small nanoparticles (Fig. 8a). The particle size-dependent decay from $^4I_{11/2}$ to $^4I_{13/2}$ favors the population of red emission state $^4F_{9/2}$ and hinders the population of green emission states $^4S_{3/2}$ and $^2H_{11/2}$. Thus, the proportion of red emission in UC fluorescence gradually increases as the particle size decreases (Fig. 8b). Similar color change phenomena induced by the particle size were found in various Ln UCNCs.[108]

Besides manipulating the synthesis conditions, high-temperature post-treatment on the as-prepared NCs can also increase the particle size. The second sintering in muffle furnace is often used to improve the crystallinity of the NCs and

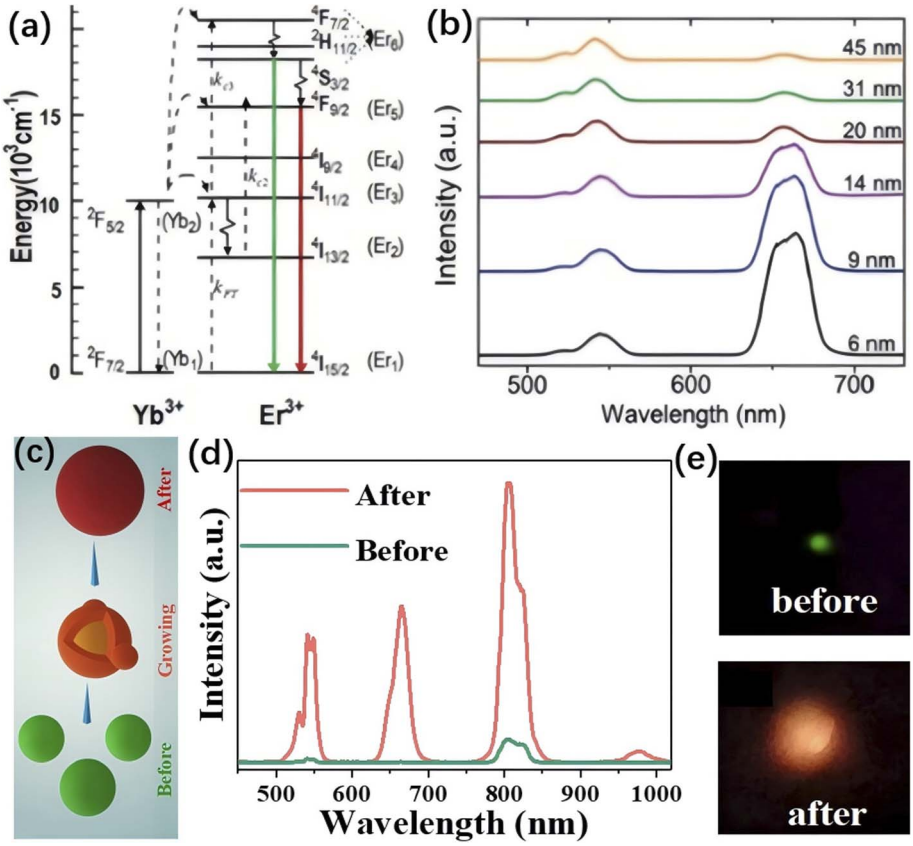

Fig. 8 Particle size-induced multicolor tuning in UCNCs. (a) Main population and luminescence pathways related to UC emission in $NaYF_4$:Yb/Er NCs. (b) Room temperature UC emission spectra of $NaYF_4$:Yb/Er NCs with sizes ranging from 6 nm to 45 nm. The spectra are normalized to the Er^{3+} emission at 540 nm.[107] Copyright 2012, Royal Society Chemistry. (c) Schematic diagram of regrowing process aroused by laser annealing. (d) UC spectra of the as-prepared NCs and post-annealed NCs under identical excitation (1530 nm, 50 mW cm^{-2} 100 mW cm^{-2}). (e) Digital photographs of the visible lights of the as-prepared NCs and post-annealed NCs. Reproduced with permission.[109] Copyright 2019, IOP.

enlarge the particle size. In a typical procedure, hundreds of degrees centigrade and several hours are needed. Compared to furnace heating, laser annealing is more convenient and also a feasible way to evidently enlarge the particles. On the basis of the light-to-heat conversion, once the temperature is beyond some reaction threshold, particle start to grow and become bigger. Due to traditional NCs with low conversion efficiency of light-to-heat, laser annealing usually requires high incident power density and long treatment duration.[8]

Liu's group developed a facile, ultrafast, and low-threshold laser annealing strategy, utilizing Er^{3+} heavily doped UCNCs with highly efficient light-to-heat conversion upon 1530 nm excitation. This technique can increase the particle size from 8 to 14 nm within only ~25 s, the growth mechanisms are illustrated in Fig. 8c.[109] It is revealed that the as-prepared 80 mol% Er:$NaGdF_4$ UCNCs emit weak green light, while the post-annealed counterparts yield bright red dominant light (Fig. 8d and e). Noted that the color change direction of NCs with different sizes can be different, depending on the specific UC pathways, as evidenced by the opposite changes observed in low Er^{3+} doped NCs upon 980 nm excitation[107] and high Er^{3+} doped NCs upon 1530 nm excitation.[109,110]

3.1.5 Building core–shell structure. C–S architecture is one of the most important techniques to improve the performance of nanomaterials. For Ln UCNCs, an additional shell is often fabricated outside the core particle, forming the surface passivation through building the C–S structure. The surface passivation of UCNCs includes the coating/epitaxial growth of a homogeneous or heterogeneous inert shell. The homogeneous inert shells are typically LnF_3@LnF_3,[59] $NaLnF_4$@$NaLnF_4$,[60] and $LiLnF_4$@$LiLnF_4$,[61] while the heterogeneous inert shells are typically cubic $NaLnF_4$@CaF_2,[62] NCs@SiO_2,[63] and NCs@PVP.[64] In addition to the inert shell, an active shell with Yb^{3+} dopant was first found to be more effective for improving the luminescence intensity,[111] and the role of active shell is to increase the absorption rather than the luminescent quantum yield.[112]

Above C–S structures are mostly utilized for either higher luminescence efficiency or better biocompatibility, the emission color, however, can be sometimes altered. Importantly, the effects of C–S structures on the UC color should be more effective than that of the particle size, since surface passivation can largely eliminate the surface quenching by thick coating while the increase of the particle size only suppresses it.

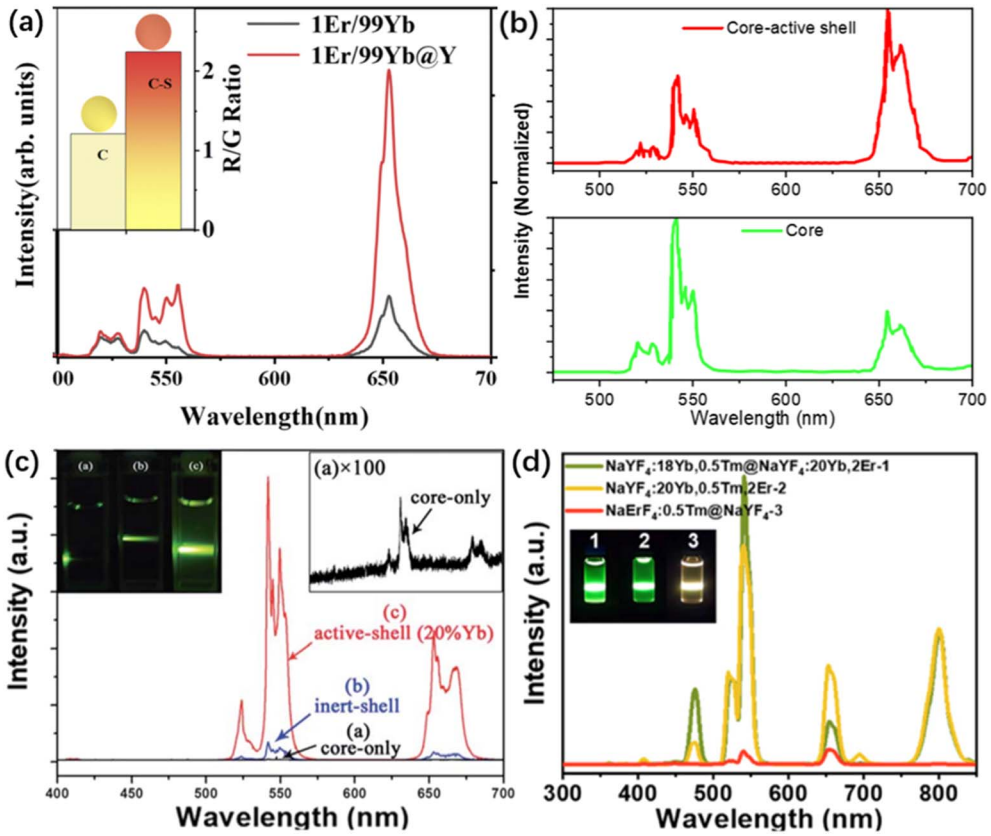

Fig. 9 C–S structure-induced UC color change. (a) Inert shell-induced,[81] Copyright 2021, American Institute of Physics. (b) Sensitizer doped active shell-induced, reproduced with permission.[113] Copyright 2015, Royal Society Chemistry. (c) Counterexamples showing the substantially unchanged UC color with inert shell and active shell coatings,[114] Copyright 2015, Royal Society Chemistry. and (d) activator doped shell-induced UC color change.[83] Copyright 2022, American Chemical Society.

Zhou *et al.* investigated the effects of inert shell on the UC intensity and color, using $NaYbF_4$:1Er core-only and $NaYbF_4$:1-Er@$NaYF_4$ C–S NCs for comparison. As shown in Fig. 9a, the green and red emissions are comparable in intensity for core-only UCNCs, while the red emission becomes dominant after coating an inert shell.[81] As for the sensitizer ions enriching active shell, it can also greatly alter the UC emission color. As demonstrated in $NaYF_4$:Nd/Yb/Er@$NaYF_4$:Nd/Yb UCNCs upon 808 nm excitation, the growth of $NaYF_4$:Nd/Yb active shell changes the red to green intensity ratio significantly (Fig. 9b).[113] Noted that the additional layer, no matter for inert shell or active shell, does not necessarily alter the UC color (Fig. 9c),[114] indicating the complex mechanisms of UC luminescence.

The observed color changes upon shell coating arise from mechanistically distinct effects of inert and active shells. For the inert-shell case (Fig. 9a), epitaxial passivation reduces surface-related non-radiative decay channels and suppresses high-energy multiphonon relaxation; because green-emitting levels (*e.g.*, $^2H_{11/2}$, $^4S_{3/2}$ in Er^{3+}) are generally more vulnerable to surface quenching and multiphonon loss than the lower-energy red-emitting $^4F_{9/2}$ level, surface passivation often leads to a relative enhancement of red emission (increased R/G ratio).

In contrast, an active shell doped with sensitizers (*e.g.*, Yb^{3+}, Nd^{3+}) introduces additional absorption and new interfacial ET channels that can preferentially populate specific emitting levels in the core; depending on the shell composition and pump wavelength, such shell → core ET may favor population of higher-lying green levels and thus shift the apparent color toward green (Fig. 9b). It should be emphasized that whether color changes occur depends on the balance between (i) suppression of surface quenching, and (ii) the addition of shell-mediated ET pathways-which explains why some coatings do not appreciably change the UC color (Fig. 9c).

However, it is clear that the C–S architecture can add other Ln activators and additional emission bands for the core NCs, and therefore change the emission color. As evidenced by the core–shell structured $NaYF_4$:Yb/Tm@$NaYF_4$:Yb/Er NCs, the construction of another luminescent shell adds strong green emission, which overwhelms the original blue light from the core (Fig. 9d).[83] Based on the multicolor core–shell UCNCs, the barcoding in single UC microcrystals is demonstrated. Zhang *et al.* utilized a layer-by-layer epitaxial growth route to add differently composed tips on a microrod, ultimately formed a series of dual-color microrods among the R/G/B components, achieving the barcoding with ultrahigh resolution. This approach not only improved the color contrast of precursor microrods but also guided the multicolor tuning to the single microcrystal level.[44]

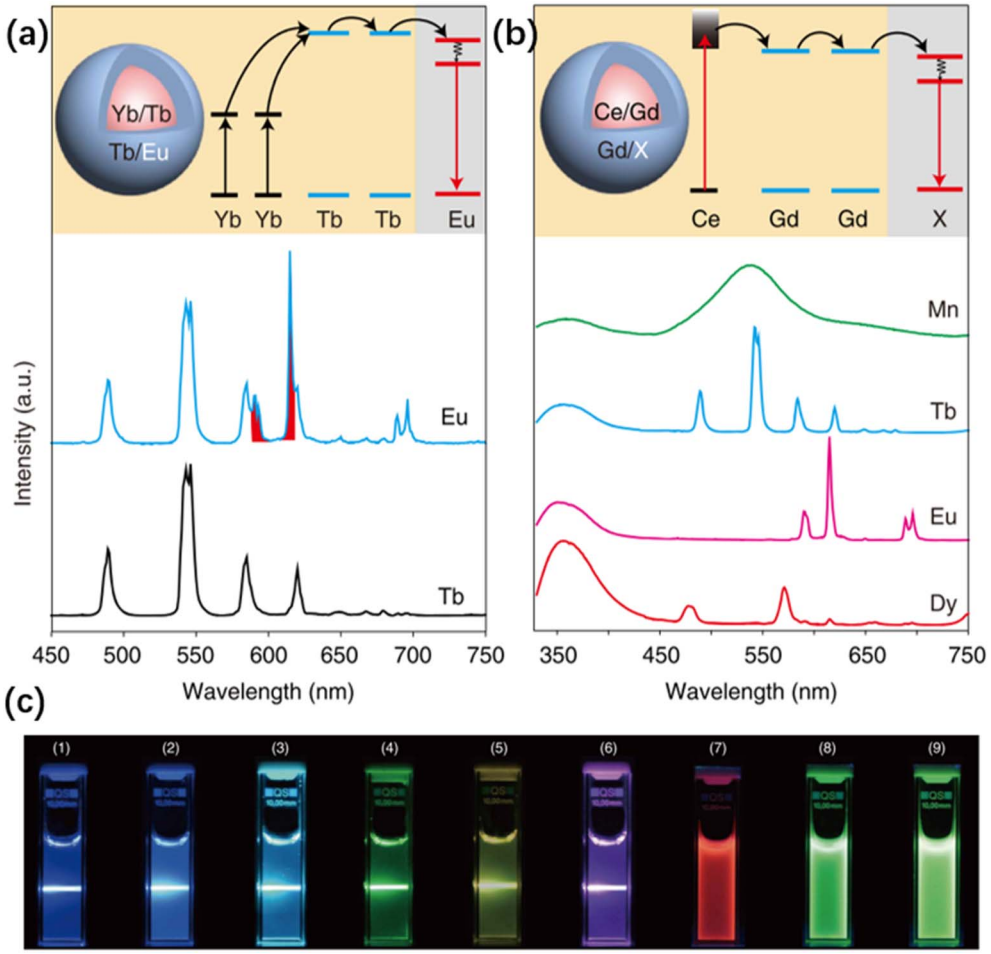

Fig. 10 Multicolor tuning *via* cation exchange. (a) UC emission spectra before and after treatment of $NaYbF_4$:Tb@$NaTbF_4$ NCs by $EuCl_3$, excited at 980 nm. (b) DS emission spectra of $NaGdF_4$:Ce@$NaGdF_4$ NCs treated by $MnCl_2$, $TbCl_3$, $EuCl_3$, and $DyCl_3$, excited at 254 nm by an ultraviolet lamp. (c) Luminescent images of the corresponding colloidal solutions.[65] Copyright 2016, Springer Nature.

3.1.6 Exchanging the surface cations. Cation exchange is a chemical reaction process in which the adsorbent materials replace their cations in a solution or gas with other cations of the same charge, resulting in the removal of cations from the solution or gas. This process is commonly used in waste water treatment and various other applications to remove undesirable cations from a liquid or gas stream.

In Ln doped NCs, this method essentially involves doping another activator ion into the host lattice to modify the fluorescence emission spectra of materials. Further, the cation exchange can utilize EM processes in the lattice, and allows for convenient and precise customization of luminescence based on desired colors.[65] As shown in Fig. 10a and b, the Tb^{3+} or Gd^{3+} ions in the surface lattice of C–S NCs are replaced by other A (Eu^{3+}, Dy^{3+}, Tb^{3+}, and Mn^{2+}). *Via* ET process, Tb^{3+} and Gd^{3+} ions in the core are populated. Following the EM among Tb^{3+} or Gd^{3+} in the sublattice, exchanged A are activated and alter the emission color of NCs. Fig. 10c shows the color changes *via* different cation exchange treatments, demonstrating the high feasibility and effectiveness of the approach.

To improve the luminescent intensity of NCs after cation exchange, Guan *et al.* developed oil-phase cation exchange method. This method maintains the easy pretreatment of NCs and achieves much stronger luminescence intensity in the NCs compared to those obtained by traditional aqueous cation exchange.[115]

It can be concluded that the combination of cation exchange and ET in Ln NCs enables convenient and precise customized luminescence properties.[65,82,115] Although cation exchange can be considered as another route to build C–S structure, its lower ion exchange rate and shallow exchange depth (related to ion concentration, exchange time, and surrounding temperature) prevent it from achieving the same level of performance as achieved by the widely-used C–S architecture.

Despite all this, the advantages of ion exchange method far outweigh its limitations. Compared to shell encapsulation that capable of introducing another type of A into the NCs, this color tuning strategy has the following two unique advantages: one is the facile, fast, and low-cost implementation *via* soaking and spraying with ion exchange agents; the other is the wide

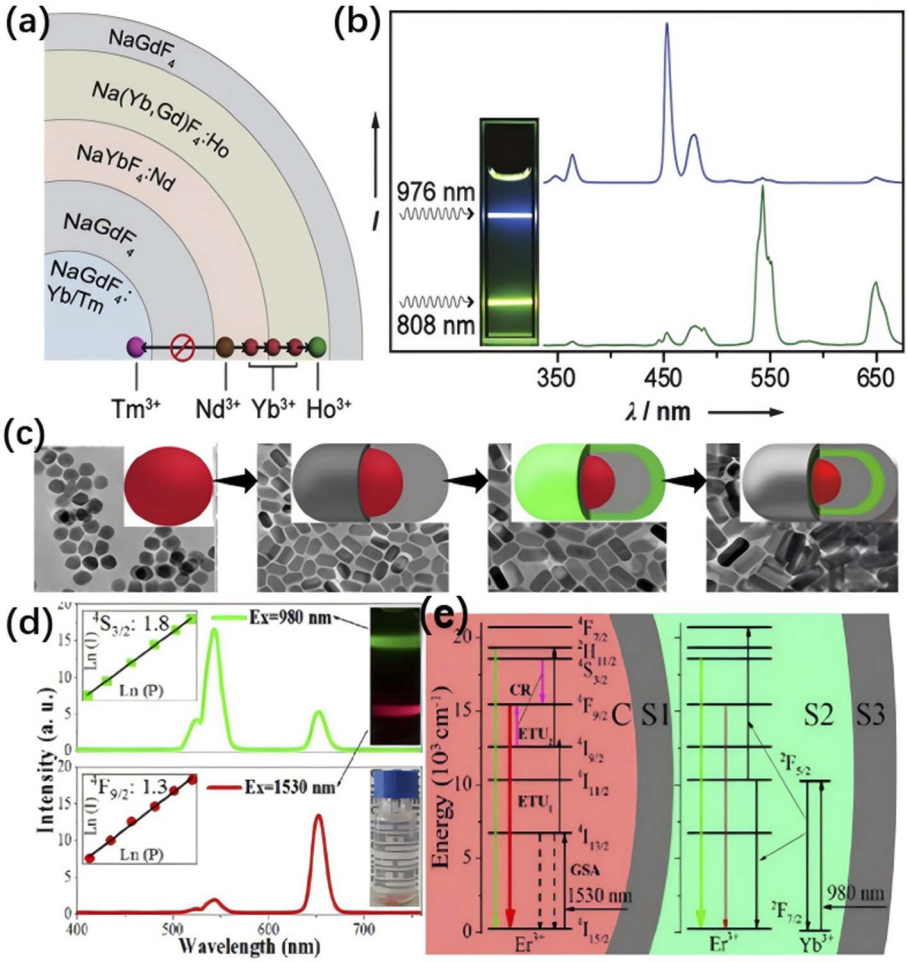

Fig. 11 Excitation wavelength-induced real-time color tuning. (a) Schematic diagram showing the structure of the formed C–S NCs. (b) The UC emission spectra as well as the luminescent images of the colloidal NCs under excitations at 976 nm and 808 nm.[119] Copyright 2013, Wiley-VCH. (c) TEM images show the corresponding structures of core, C–S, C–S–S, and C–S–S–S NCs. (d) UC spectra under excitation at 980 nm and 1530 nm. The left insets show the UC intensity as a function of excitation power in ln–ln form. Right insets are the images of the NCs dispersion and its UC luminescence in dark room upon dual-laser stimulations. (e) Energy level diagram and UC mechanism of NCs. Reproduced with permission.[120] Copyright 2020, Elsevier.

availability for various material surfaces and interfaces, and with a variety of ion exchange agents.

3.2 Real-time color tuning in ln UCNCs

The real-time color tuning is more "dynamic" that the traditional multicolor materials like organic dyes and semiconductor QDs are unavailable. The main reason is that the internal tuning nature of dyes and QDs makes it difficult to greatly change the position of spectral band in real-time,[27] which is usually slow and quite inconvenient. The unique merits of real-time color tuning can offer more dynamic platforms for applications in advanced anti-counterfeiting, photoswitching, and high-resolution bioimaging.[84,85,116–118] In this section, different real-time color tuning results will be summarized and discussed.

3.2.1 Switching excitation wavelength. Among the current strategies for real-time color tuning, the most popular one is *via* switching the excitation wavelength. The excitation wavelength-induced color-tunable UCNCs usually require construction of C–S structure. Different dopants, arranged in different layers of the C–S NCs, are responsible independently for different colors upon different excitation wavelengths. Notably, the possible detrimental interactions between neighboring luminescent layers can be eliminated by inserting an inert layer.

A pioneer real-time color tuning work was reported in 2013, a 5-layer UCNC with composition of $NaGdF_4$:Tm/Yb@$NaGdF_4$@$NaYbF_4$:Nd@$NaGdF_4$:Yb/Ho@$NaGdF_4$ was constructed,[119] shortened as Gd:Tm/Yb@Gd@Yb:Nd@Gd:Yb/Ho@Gd for the sake of simplicity, and others C–S $NaLnF_4$ NCs in this review will be abbreviated similarly. The first layer is sensitive to excitation at 976 nm and produces blue UC luminescence. The third layer absorbs excitation at 808 nm and then transfers the energy to the fourth layer, which emits mainly the green light. The second layer is inert, separating spatially the first and third layers to avoid their possible interference. The outermost layer is also inert and is used to passivate the surface quenching, thereby improving the UC intensity (Fig. 11a). The switchable UC luminescence upon different excitation wavelengths is shown in Fig. 11b.

Soon afterwards, rationally designed 4-layer Y:Nd/Yb/Tm@Y:Nd@Y@Y:Yb/Er UCNCs were prepared. The formed UCNCs emit orthogonal blue (and UV) and green light in response to excitations at 808 nm and 980 nm, respectively, capable of controlled two-way of photoswitching of spiropyran.[121] Similarly, 4-layer Gd:Yb/Er@Y@Y:Yb/Tm@Yb:Nd@Y UCNCs were prepared to realize blue and UV light upon 800 nm excitation while green light upon 980 nm excitation, and further efficiently trigger reversible photocyclization of the chiral diarylethene molecular switch.[122]

It is well-known that the biggest limitation for UCNCs is their low luminescent quantum yields, which are typically below 1%, although these internal quantum yields already neglect the weak absorption ability of Ln ions.[123] Consequently, the real-time color-tunable UCNCs are restrained by the insufficient emission efficiency of different color components. Consequently, various designs are proposed to enhance the quantum yields of the color-tunable UCNCs.

To enhance the intensity of Nd^{3+} sensitized UC emission, sandwich structure that capable of eliminating the detrimental interactions between Nd^{3+} and activators has proven to be highly effective.[124] Inspired by this, Li *et al.* built 6-layer NCs as Gd:Yb/Er@Y:Yb@Gd:Yb/Nd@Y@Gd:Yb/Tm@Y.[116] By tuning the thickness of the absorption filtration layer ($NaGdF_4$:Yb/Tm), the UCNCs exhibited two groups of independent orthogonal emissions: Tm^{3+} prominent blue UC under the excitation at 980 nm and Er^{3+} prominent green UC upon 796 nm excitation.

In addition, our group developed relatively compact 4-layer Er@Y@Y:Yb/Er@Y NCs, capable of switchable green and red UC emissions (Fig. 11c).[120] Utilizing the strong absorption at 1.5 μm of heavily doped Er^{3+} in the core as well as the passivation of the inert shell, the core of formed NCs can generate highly efficient red emission.[125] While under 980 nm excitation, the traditional Er^{3+} and Yb^{3+} co-doped layer, after coating an inert shell, emits bright green light (Fig. 11d). The corresponding mechanisms responsible for the color tuning are depicted in Fig. 11e. Additionally, the CIE coordinates remain relatively unchanged under different excitation intensities or temperature variations, indicating high color stability.

To date, the excitation wavelength-induced color tuning has been successfully demonstrated in various UCNCs, as summarized in Table 2. They basically follow the one-layer-to-one-color design, due to a single layer is usually sensitive exclusively to specific excitation and one layer emits only one color. Thus, construction of additional shell or shells to add other luminescence colors is required, especially for Nd^{3+} sensitized UC emission. In addition, an inert shell between two emissive layers is necessary to avoid their detrimental interactions. It seems that highly cumbersome structures are inevitable for bright and wide-range color tuning. For instance, to achieve two tunable colors with high performance, the NC requires at least four layers, two luminescent layers and two inert layers.[31,77] The layer-by-layer synthesis of the C–S NCs is time-consuming, high-cost, and facing the risk to phase separation, which are more evident when growing more layers. Therefore, the exploration of structurally simple and high-performance color-tunable UCNCs has become a pressing issue.

To streamline the bulky structure, our group developed a highly compact UCNCs capable of switching between green and red emissions.[126] The key to this design is build a single layer that can accordingly emit two different colors under two excitation wavelengths. UCNCs co-doped with Er^{3+} and Yb^{3+} typically emit green light when excited at 980 nm, but the addition of a small amount of Tm^{3+} significantly favors the population of red emission energy level, enabling the emission of red light under 980 nm excitation. On the other hand, under 1.5 μm excitation, the influence of Tm^{3+} is negligible due to a different energy pathway, resulting in green emission. Owing to the core itself can emit two different colors, the designed color-tunable NCs comprise only two layers. Another strategy was proposed in 2024, in which 1973 nm excitation was introduced to simplify the structure of color-tunable UCNCs. Upon 980 nm and 1973 nm synergistic excitation, green, chartreuse, yellow, orange, and red can be tuned dynamically in the $NaYF_4$:Er^{3+} single UCNC.[84]

As mentioned above, current real-time color tuning mostly demonstrates only two-color components, mainly limited by the two available excitation wavelengths at 800 nm and 980 nm.[118,127] The tunable R/G/B emissions are of vital importance for the real-time UC color tuning, due to their prospect of full color gamut. However, the implementation of R/G/B-based real-time UC color tuning is far from an easy task.

Based on the recently developed 1.5 μm excited Er^{3+}-doped NCs, in 2020, our group attempted to build R/G/B color-tunable UCNCs, using the composition of Y:Yb/Tm@Lu@Y:Er@Lu@Y:Nd/Yb/Er. The core emits blue UC luminescence upon 980 nm excitation, the Er^{3+} heavily doped layer emits red dominant luminescence upon 1530 nm excitation, and the Nd^{3+}/Yb^{3+}/Er^{3+} triply doped layer generates green light upon 800 nm excitation. However, the red component obtained is much weaker than the other two components in brightness.[126] In 2021, much improved R/G/B color tuning was successfully achieved in 7-layer UCNCs with composition of Yb:Tm@Gd@Gd:Yb/Er@Y:Nd/Yb@Gd@Er:Tm@Gd. In these UCNCs the Yb:Tm core, Gd:Yb/Er@Y:Nd/Yb layers and Er:Tm layer are responsible for blue, green, and red emissions upon 980 nm, 800 nm and 1530 nm excitations, respectively.[29] This design improved the red component through the high doping Er^{3+} and the condensation effects of trace Tm^{3+}. Very recently, they proposed an updated 7-layer UCNC of Er:Tm@Y@Y:Yb@Lu:Nd/Yb@Y@Yb:Tm@Y. Utilizing the diffusion of Er^{3+} dopants from core to the two neighboring shells, the $NaYF_4$:Yb layer is actually $NaYF_4$:Yb/Er, and therefore this UCNC is capable of emitting tunable R/G/B light.[128] Other structures were adopted to generate tunable R/G/B emission upon 800 nm, 980 nm, and 1530 nm. For instance, 7-layer UCNCs with composition of Y:Yb/Tm@Y:Yb/Nd@Lu@Y:Yb/Er@Lu@Er:Tm@Lu[28] and 6-layer UCNCs of Y:Yb/Tm@Y@Y:Er/Tm@Y@Y:Nd/Yb/Er@Y:Nd[85] both demonstrated successfully the real-time R/G/B color tuning ability.

3.2.2 Altering excitation pulse width. Another strategy for real-time color tuning is to use pulsed excitation and vary the pulse parameters. The color tunability of certain NCs can be

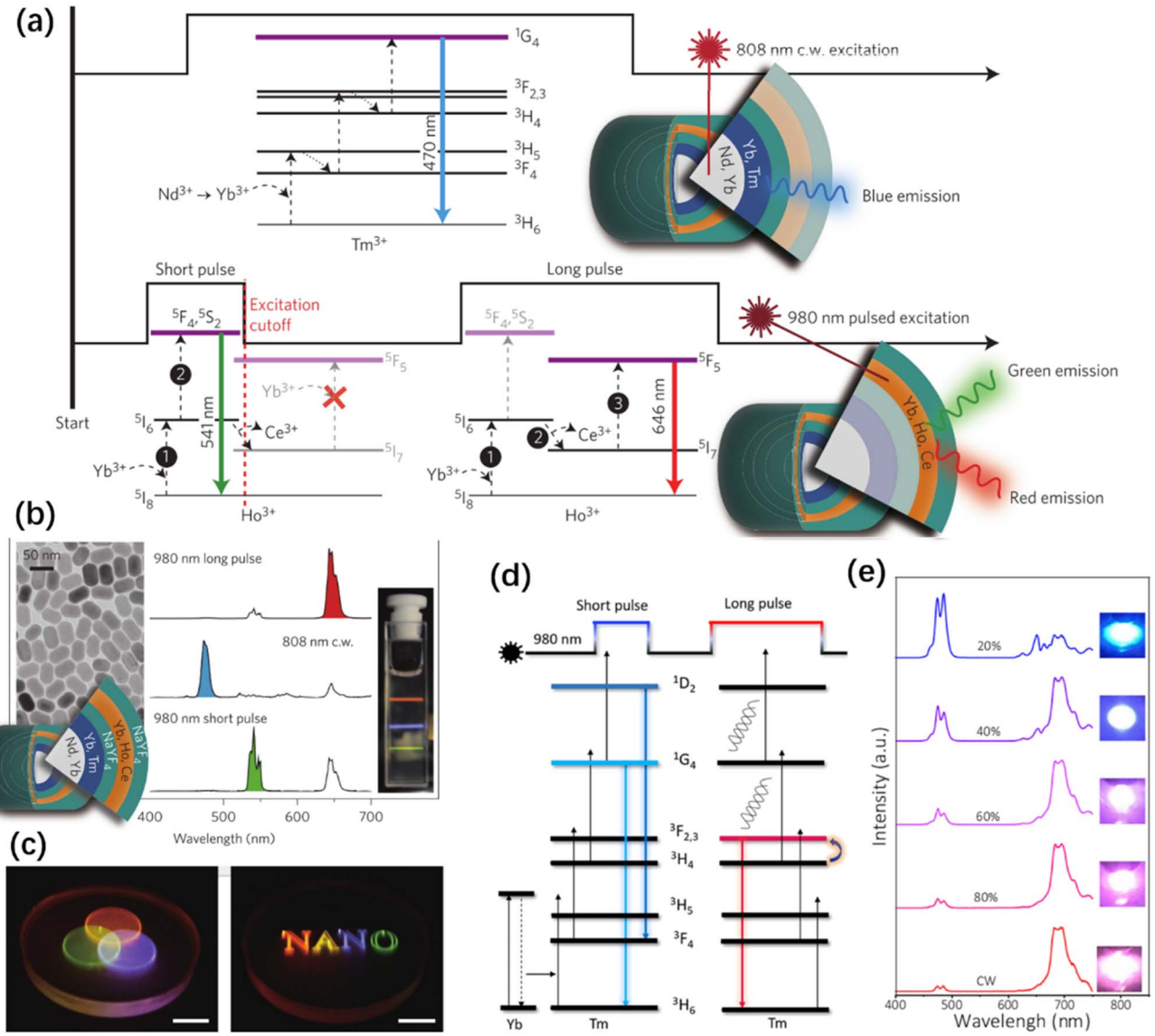

Fig. 12 Excitation pulse-induced real-time color tuning. (a) Schematic illustration of the UC mechanism responsible for the tunable R/G/B emissions. (b) Design of the UCNCs that can emit tunable colors when illuminated with NIR lasers, as shown by the emission spectra and the luminescent image. (c) Demonstration of the three-dimensional color display using the formed UCNCs.[35] Copyright 2015, Sprinter Nature. (d) Proposed color tuning mechanisms of Y_2O_3:Yb/Tm NCs under short and long pulse excitations. (e) UC spectra of Y_2O_3:Yb/Tm NCs excited by different pulse widths. Inset shows the corresponding luminescent images.[6] Copyright 2022, Optical Society America.

controlled through non-equilibrium UC processes, which is due to the varied population times of different energy levels.

In 2015, Deng *et al.* demonstrated that through the CR between Ho^{3+} and Ce^{3+}, which requires some time to occur, the long pulse 980 nm excitation can activate the red emission of Ho^{3+}. While short pulse excitation is too fast to activate efficient CR between Ho^{3+} and Ce^{3+}, resulting in green dominant UC emission (Fig. 12a). Further, combining this excitation pulse-induced green/red color tuning as well as the excitation wavelength-induced color tuning, the 5-layer R/G/B tunable UCNCs were built and the following full-color display applications were demonstrated (Fig. 12b and c).[35] In addition, many other groups have demonstrated excitation pulse-induced color tuning phenomena in various materials. Avram *et al.* achieved two independent colors, with R/G values of 0.18–0.96, from $NaGdF_4$:Mn/Yb/Er by pulse modulation.[129] Naruke *et al.* demonstrated green and red color tuning of $NaNbO_3$:Er/Yb/Al phosphors with different excitation pulse widths ranging from 50 to 2400 μs.[130]

From the above, the excitation pulse-induced UC color tuning generally originates from Er^{3+} or Ho^{3+}, and thus the color components are mainly red and green. This is due to the green and red emissions being generated from relatively close energy levels, enabling the easier manipulation of the population pathways to make one of them dominant. To introduce the blue component in the pulse-induced color tuning, Tm^{3+} is the most promising candidate as Tm^{3+} exhibits both blue and red emissions within the visible region.[131] But unfortunately, it is quite

difficult to achieve the blue and red color tuning from Tm^{3+} *via* pulse excitations, due to the red emission and the main blue emissions originate from an identical energy level of $^1G_4$. For instance, Gao *et al.* investigated the color change of LaF_3:Tm NCs, but only NIR and blue color tuning was shown by adjusting the pulse width.[132]

After that, our group demonstrated blue and red tuning in Y_2O_3:Tm/Yb NCs. The mechanism involves significant heat accumulation during long pulse and strong excitation, which quenches the traditional blue emission of Tm^{3+}. In stark contrast, $^3F_{2,3}$ levels can be strongly populated by the downward decay from upper levels, associated with the thermalization of long-lived $^3H_4$ level (Fig. 12d). Thus, these NCs can emit blue light under short pulse 980 nm excitation and red light under long pulse excitation (Fig. 12e).[6] Noted that although pulse width-induced color tuning showing good performance, additional modulation models are required, increasing the equipment cost and the operation complexity. Subsequently, color-switchable UC luminescence was achieved in a $NaYF_4$:Gd@$NaYbF_4$:Tm@$NaYF_4$ sandwich nanostructure, based on the short temporal delay for the occurrence of cross relaxation process.[36]

Additionally, a variety of new mechanisms based on pulse width modulation have emerged. For instance, the dynamically regulating green and red UC luminescence in $NaGdF_4$:Yb^{3+}/Ho^{3+}/Ce^{3+}/Sc^{3+} reported in 2024, whose mechanism primarily stems from the controlled depletion of the Ho^{3+} $^5I_6$ energy level.[133] Very recently, excitation pulse induced UC color, again green and red, was achieved based on the time-consumed back ET process from Er^{3+} to Yb^{3+} in 1 mol% Er^{3+} doped $NaYbF_4$ UCNCs.[134]

3.2.3 Adjusting ambient temperature. This section mainly summarizes another real-time color tuning strategy, which involves changing the luminescent color of Ln UCNCs by adjusting the environmental temperature. As a basic physical parameter, temperature plays an important role in every research field, mainly due to temperature can directly or indirectly affect the properties of materials and their behaviors. For Ln-based luminescent NCs, ambient temperature is closely related to the vibration of host lattice, and thus can change the rates of all the phonon-assisted processes. These phonon-assisted processes include the absorption with energy mismatch, the ET between two ions with poor spectral overlap, and the nonradiative decay from higher level to its neighboring lower level.[135] Consequently, the luminescent intensity, lifetime, and color of Ln based NCs can be tuned by the ambient temperature.

As compared to the luminescent intensity and lifetime, unfortunately, the luminescent color of Ln UCNCs seems to be less sensitive to temperature. For the most widely-used Er^{3+}

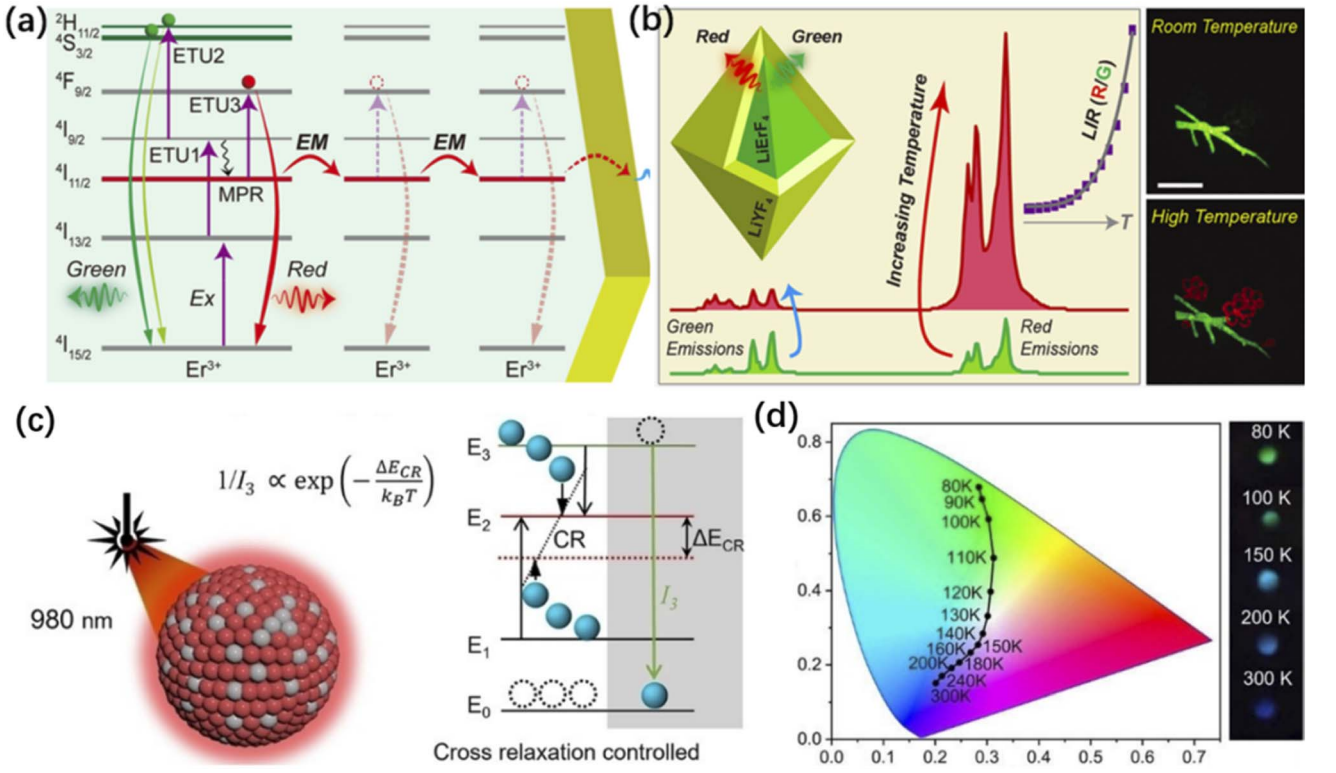

Fig. 13 Real-time color tuning by ambient temperature. (a) The mechanisms of temperature-induced color tuning *via* the competition between upward transitions and EM processes at Er^{3+} intermediate $^4I_{11/2}$ state. (b) The UC spectra of the designed $LiErF_4$@$LiYF_4$ NCs under room temperature and high temperature, right images show the thermal-induced information identification applications.[67] Copyright 2022, American Chemical Society. (c) Schematic illustration of upconversion thermal response in the Er^{3+}-rich core–shell system, the PL intensity has an exponential relation with temperature. (d) CIE chromaticity diagram of emission colors for the UCNCs at various temperatures. The beside photographs show the emission colors of UCNCs powder under different temperatures.[87] Copyright 2023, Wiley-VCH.

based UCNCs, Lojpur *et al.* revealed that raising the ambient temperature from 10 to 300 K only slightly change the UC color, the green emission band always dominates the spectra.[86] In addition, for higher temperature range of 320–470 K the intensity ratio of green and red emission of Er^{3+} still varies not evidently.[136] Similar weak effects of temperature on the luminescent colors of Ho^{3+} and Tm^{3+} are observed elsewhere.[137,138]

To improve the thermal sensitivity of UC color, heavily doped $LiErF_4$@$LiYF_4$ C–S NCs were built very recently, showing greatly changed emission color with temperature.[67] This work balanced the upward ETU and EM mediated surface quenching, maintains relatively bright light and ultra-high thermal sensitivity (Fig. 13a). Fig. 13b shows the changes in emission spectra of the samples, which exhibit green- and red-dominant light at room temperature and high temperature, respectively. As a result, this thermochromic material shows great potentials in the fields of anti-counterfeiting and information identification (insets of Fig. 13b). It seems that the highly-doped activator is of vital importance for enhancing the thermal sensitivity of UCNCs. Very recently, Y:75Er@Y C–S NCs exhibited evident change of their UC emission color, within the cryonic region. As depicted in Fig. 13c, the phonon-assisted CR processes, that quench the green emission (E_3) and meanwhile favor the red emission (E_2), can be greatly suppressed under low temperature. Thus, the decrease of ambient temperature leads to the significantly enhanced green emission as compared to red emission. After introducing another blue luminescence layer which is not very sensitive to the temperature, forming the Y:75Er@Y@Y:75Yb/2Tm@Y core–multishell UCNCs, the emission color upon 980 nm excitation can be tuned from blue to green, with decreasing the ambient temperature (Fig. 13d).[87]

Therefore, by controlling the environmental temperature, it is possible to dynamically manipulate the luminescence color of NCs, providing a new approach for their applications in areas such as biological imaging and sensors.[139,140] Notably, the main drawback of this strategy is that environmental temperature changes are usually not very rapid, especially for the cooling process, making it somewhat lagging compared to other real-time color tuning methods.

3.2.4 Tuning excitation intensity. Among all the real-time color tuning strategies, the most convenient one might be based on the change of excitation intensity (power density), as this method possesses easy operation and fast response, and does not require additional excitation equipment or chemical treatments of NCs.

A pioneering work was reported in 2010, aiming at the "remote-control" photoswitching applications.[24] Using Er^{3+}/Yb^{3+} and Tm^{3+}/Yb^{3+} ions doped C–S–S $NaYF_4$ NCs, at high power densities of 980 nm excitation, the dominant emissions are ultraviolet and are appropriate to drive the ring-closing, forward reactions of dithienylethene photoswitches. The visible light generated from the same NCs upon weak excitation triggers the reverse reactions and regenerates the original photoisomers. However, the color purity of the formed NCs is relatively low, and the color tuning showed switchable green and UV dominant emissions, with one component beyond the visible region.

Inspired by this convenient and versatile method that can regulate spatially and temporally the photochemical reactions,

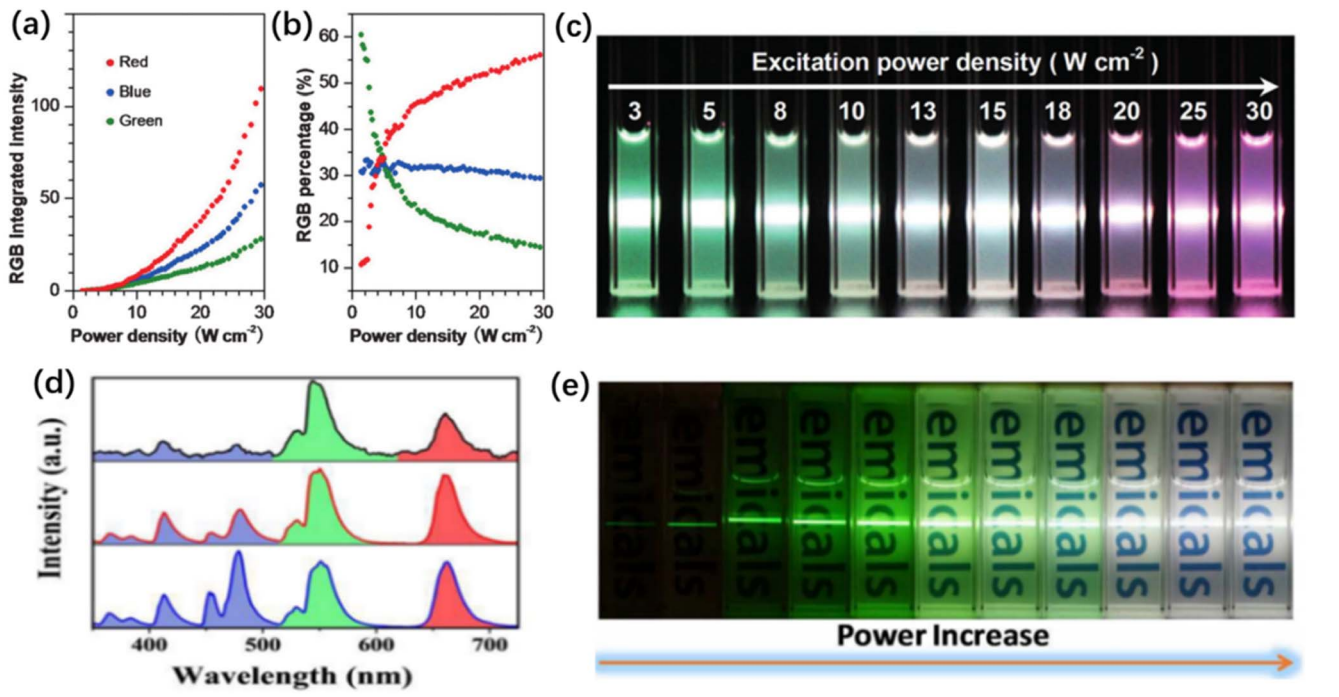

Fig. 14 Real-time color tuning by excitation intensity. The (a) integral intensities and (b) fractions of different color emissions with the excitation intensity of Gd:Yb/Tm/Er@Gd:Eu@Y NCs, and (c) shows the corresponding color evolution.[141] Copyright 2015, Wiley-VCH. (d) UC spectra of Gd:Er@Gd@Gd:Tm@Gd NCs upon 980 nm excitation using power densities of 5 W cm^{-2} (top), 12 W cm^{-2} (middle), and 19 W cm^{-2} (bottom). (e) UC luminescent images of the NCs dispersion under excitation power density increasing from 5 to 19 W cm^{-2}.[142] Copyright 2016, Royal Society of Chemistry.

other excitation intensity-dependent color-tunable NCs were developed. For instance, Li *et al.* prepared Y:Yb/Tm@Y@Y:Yb/Er@Y C–S–S–S UCNCs and demonstrated their applications of noninvasive and reversible cell adhesion and detachment *via* 980 nm laser mediated photoisomerization.[25] In 2015, Gd:Yb/Tm/Er@Gd:Eu@Y C–S–S NCs was built towards the color display application, which is clearly a promising and applicable field for the color-tunable UCNCs. The combination of multiple narrow spectral bands results in the emission of white light, and importantly, the emission colors can be tuned by changing the excitation power density (Fig. 14a–c).[141] Later on, 4-layer Gd:Yb/Er@Gd@Gd:Yb/Tm@Gd NCs was constructed, achieving green ↔ white color tuning upon a single excitation at 980 nm, using different power densities (Fig. 14d and e). Specifically, the proportions of blue and red emissions increased from 6% and 22% to 54% and 23%, respectively, while that of green emission decreased from 70% to 24%.[142] In 2024, a mixture of $NaYF_4$:Er/Ho@$NaYF_4$ and $NaYbF_4$:Tm@$NaYF_4$ NCs demonstrated a wide-range of color tunability, from blue to red and yellow, by simply altering the intensity of 980 nm excitation.[143]

So far, the excitation intensity-induced color tuning generally demonstrates only the change between two color components. Achieving high-quality R/G/B color tuning through a single wavelength is highly promising and remains a formidable challenge.

Very recently, we for the first time demonstrated that it is possible to achieve tunable R/G/B UC luminescence using a single excitation wavelength, on the basis of the photon-order dependent UC nature. A relatively compact C–S–S NC was synthesized, with rational designed compositions of Er/Yb and Tm/Yb in the core and the outermost shell, respectively. By increasing the power density of the 980 nm excitation laser, the emitted light color from the formed NCs evolved as green → red → blue, corresponding to 2 → 3 → 4-photons processes involved in the UC luminescence.[144]

Despite all the excellent advantages of excitation intensity-induced color tuning, the uneven brightness of different color components, as well as the single-path of color change restricts its potential value in specific applications like full-color display.

4. Applications of color-tunable Ln UCNCs

Ln based color tuning is characterized by the high stability, well-controlled emission, and wide versatility. Combining these features with the unique merits of UC luminescence like large anti-Stokes shift and deep penetration to biological tissues, the color-tunable UCNCs can be useful in numerous fields. This section will summarize the applications of color tuning in UCNCs, but noted that the color displaying is not included, even though it is the most evident application for color-tunable UCNCs. The main reason is that the performance indicators of current color-tunable UCNCs are still far from meeting the actual demands of color display devices.[29,35,128]

4.1 Anti-counterfeiting

There are many promising applications for color tuning using Ln^{3+}-doped UCNCs, with the most widespread being fluorescence anti-counterfeiting. Anti-counterfeiting technology is a technology adopted to prevent piracy and fakes, which can accurately distinguish authenticity within a certain range and is not easily imitated and replicated. Fluorescence anti-counterfeiting techniques are particularly important in the age of information, where protecting and displaying information is crucial, such as color-changed labels on products, advanced hidden symbols on currency, anti-counterfeiting barcodes for traceability, and high capacity dynamic QR codes for electronic login. The ability of the color-tunable UCNCs offers a new class of optical materials ideal for multilevel authentication against product counterfeiting. In addition, Ln^{3+} UCNCs can be combined with other nanomaterials like magnetic nanoparticles and QDs, to form nanocomposites, making the fluorescence anti-counterfeiting technology more diverse.[145–147]

Fluorescence anti-counterfeiting often utilizes both temporal and spatial dimensions, achieved by different ways including encrypted fluorescence patterns, overlapping of different fluorescence layers, changed fluorescence pattern over time, and combinations of above ways.

In the encrypted fluorescence patterns, the Ln^{3+} doped UCNCs can be multicolor or real-time tunable. As shown in Fig. 15a, the hidden patterns printed and hand written on the banknote are invisible under normal circumstances, while it appears under irradiation of UV light. However, this type of anti-counterfeiting is easy to copy, as the hidden pattern can be visualized by using many other DS phosphors. This means conventional security inks have a limited capacity for information storage or complexity to prevent counterfeiting. Owing to the color tuning ability of Er:2Eu@Y@Yb:0.5Tm@Y NCs *via* the ingeniously designed composition and arrangement, the hidden pattern not only appears but also exhibits different colors with increasing the excitation power of 980 nm laser, which highly ameliorates the security level of this anti-counterfeiting technique.[148]

For the overlap of different fluorescence layers, multicolor UCNCs are often adopted. A QR code was prepared by the aerosol jet printing technique with overlapped fluorescence layers in 2012 (Fig. 15b).[149] Green UC ink was used to print QR codes on paper and transparent tape, and blue UC ink was utilized to create embedded security characters. These QR codes, along with the tiny hidden characters, were not visible and unreadable under normal lighting. However, they are clearly discernible when illuminated with a 980 nm continuous-wave laser, which provided high-safety QR codes. After that, a high security, high-throughput, user-friendly, designable, and low cost 3-layer QR using UCNCs was developed (Fig. 15c).[150] Printing inks containing UCNCs with red, green, and blue light emissions were separately fabricated, and were further utilized for full color printing *via* controlling the overlap of the three-color inks. As a result, this multilayer printing and splitting technology can significantly increase the information storage capacity compared with 2D QR codes.

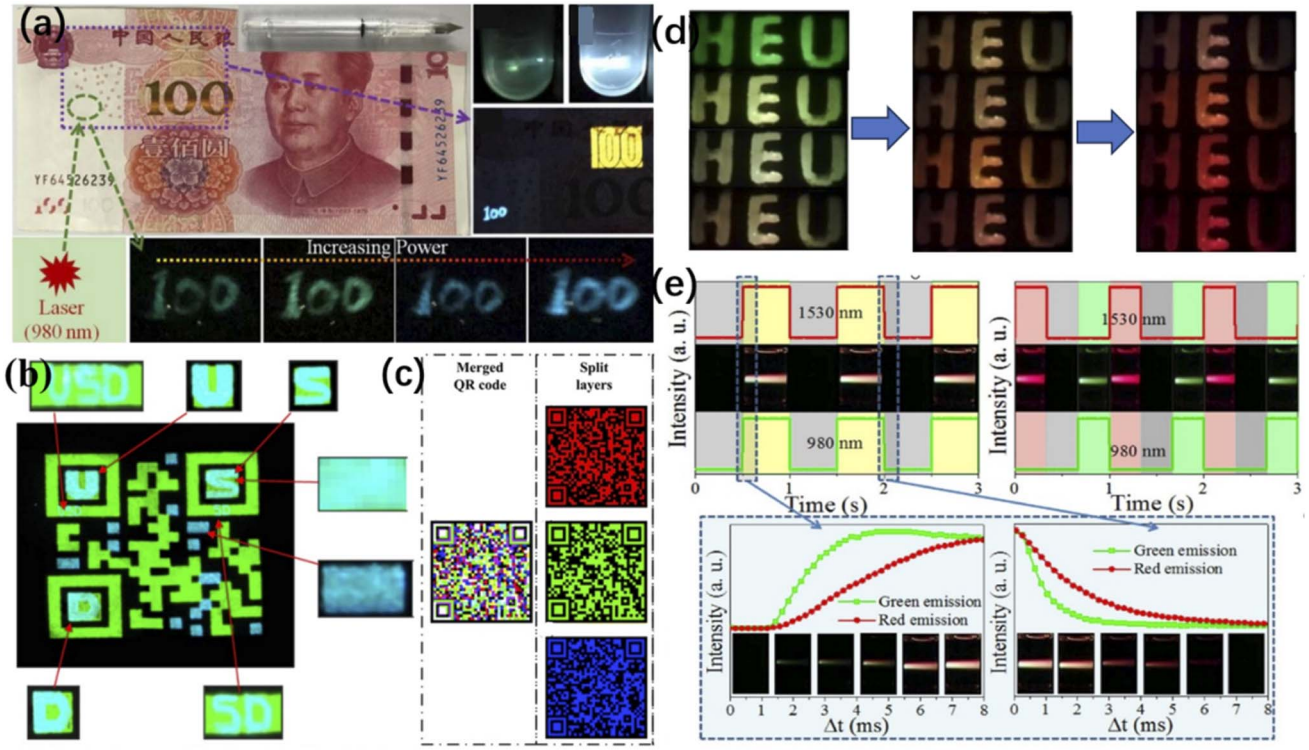

Fig. 15 Demonstrations of the anti-counterfeiting using color-tunable UCNCs. (a) Normal banknote of China with a hand-written '100' in the green circle region, which is invisible under sunlight while becomes visible and appear as different color under UV lamp illumination and variable powered 980 nm laser excitation.[148] Copyright 2019, Royal Society Chemistry. (b) UC image of QR code which was inserted by several characters with blue UC ink.[149] Copyright 2012, IOP. (c) 3D QR code merged by three-color QR codes, which can be extracted through R/G/B color channels.[150] Copyright 2016, Royal Society Chemistry. (d) Demonstration of steady-state anti-counterfeiting using color-tunable NCs. (e) Demonstration of non-steady-state color tuning under synchronous and asynchronous excitations. The bottom illustrates the detailed evolution of color changes within the rising and falling edges.[151] Reproduced with permission. Copyright 2020, Elsevier.

As for the changed fluorescence pattern over time, real-time color-tunable UCNCs are more proper, as the security ink demonstrated by Liu's group.[151] This anti-counterfeiting technique can utilize both steady and dynamic color tuning. As shown in Fig. 15d, the color-tunable NCs dispersion was sprayed onto a concave mold with a 'HEU' pattern. Under dual excitation at 980 nm and 1530 nm with different power ratios, the emission color gradually changed from green to red. Similar anti-counterfeiting demonstrations based on the real-time color-tunable UCNCs can be found elsewhere, but *via* either different excitation duration or ambient temperature.[33,152] For dynamic color tuning-based anti-counterfeiting, when excited synchronously by two pulsed lasers, no light and yellow-green light appeared sequentially, while asynchronous excitation resulted in a cycle of no light → green light → red light, demonstrating its excellent anti-counterfeiting ability (Fig. 15e). Furthermore, the green and red UC emissions have relatively long and varied rising/decay times. As a result, the frame-by-frame synchronous excitation revealed that the NCs emitted green light first and then yellow, while the extinction process showed yellow light before turning red (bottom of Fig. 15e).

Using a synergic way combining NCs composition, excitation manner, and excitation wavelength, Mn^{2+}-activated C–S UCNCs with short- and long-lived emissions were fabricated towards multilevel anti-counterfeiting application.[153] It is revealed that a steady irradiation with a 980 nm laser leads to multicolor patterns displaying characteristic emissions of Ln^{3+} and Mn^{2+}. In contrast, dynamic scanning of the same patterns with a focused laser beam yielded different emission patterns. More importantly, the color output of the main spot emission can be varied from red to white by controlling the doping composition. In addition, using excitation at 808 nm resulted in emission features that are comparable to those obtained on 980 nm excitation. Above demonstrations indicate the comprehensive anti-counterfeiting ability of these color-tunable NCs at different time resolutions.

4.2 Temperature sensing

Temperature is an essential factor in natural world where numerous activities are temperature dependent. Especially, monitoring the temperature in small area is of vital importance for understanding and further utilizing these microscopic thermal processes. Most of traditional temperature sensors are contact thermometers, where the thermal reading is achieved by direct physical contact of the probe with the body in which the temperature should be determined, based on the thermal equilibrium condition.

Compared to traditional temperature measurement techniques, Ln-based UCNCs fluorescence thermometry is particularly needed owing to its non-contact nature and unique photoluminescence properties.[102] For example, Ln-based UCNCs

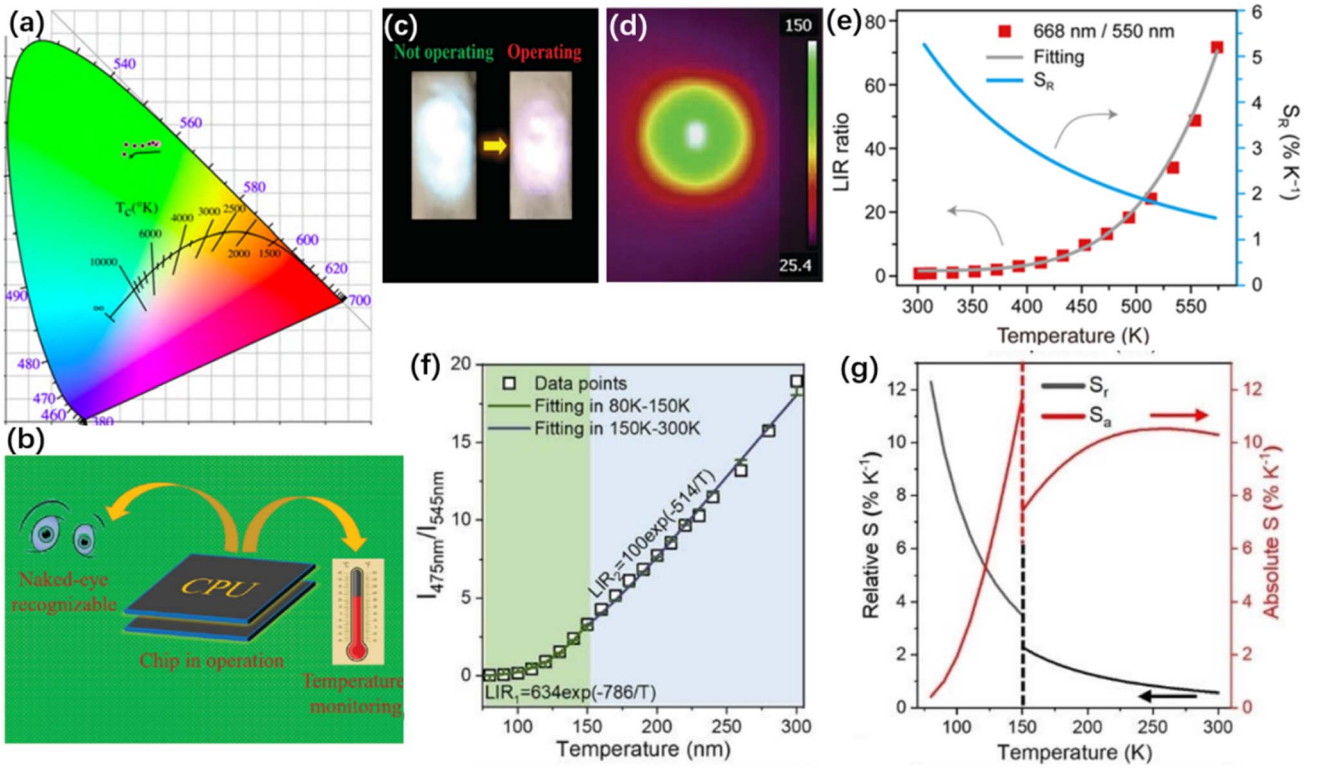

Fig. 16 Temperature sensing using the color-tunable UCNCs. (a) CIE 1931 chromaticity diagram of $Na_5Gd(WO_4)_4$:Tb/Er/Yb at various temperature under 980 nm excitation.[159] Copyright 2020, Elsevier. (b) and (c) Real-time temperature monitoring of a chip in operation *via* visual color alteration of the $NaYF_4$:Yb/Ho/Tm UC nanowires. (d) Thermal images of the UC nanowires at 150 °C using an infrared thermal imager.[161] Copyright 2019, Royal Society Chemistry. (e) FIR values and corresponding relative sensitivities of the Er^{3+} UC emissions from $LiErF_4$@$LiYF_4$ C–S NCs under excitation at 1530 nm.[67] Copyright 2022, American Chemical Society. (f) FIR and corresponding fitted curves of Y:75Er@Y@Y:75Yb/2Tm@Y core–multishell UCNCs. (g) Relative and absolute sensitivity of the core–multishell UCNCs.[87] Copyright 2023, Wiley-VCH.

can be used to measure temperature deep inside biological tissues with micro and nanoscale spatial resolution, which is highly useful for disease diagnosis and phototherapy.[154,155] In optical thermometry, temperature readout is often through optical parameters such as the emission intensity, lifetimes, spectrum shift, and spectrum bandwidth.[156] Especially, the extraction of thermal knowledge can be achieved by the fluorescence intensity ratio (hereafter FIR) of thermally-coupled levels, based on a Boltzmann-type distribution.[157] Currently, FIR thermometry is widely used in temperature measurement applications *via* UCNCs.[158] The main benefit of this class of luminescence nanothermometry is its independency of signal losses and possible fluctuations in the excitation intensity.[159]

Unfortunately, the sensitivity of thermally-coupled thermometry is relatively low, because it is proportional to the energy gap but a relatively small gap is the prerequisite for thermal coupling of two levels. The non-thermally-coupled levels, with large energy gap and usually emitting different colors, are therefore adopted to pursue higher sensitivity. Clearly, the temperature-induced color-tunable UC materials are perfect candidates for non-thermally-coupled thermometry.

In 2019, $Na_5Gd(WO_4)_4$:Tb/Er/Yb phosphors were synthesized as the sensing probes. The Er^{3+} was introduced to enhance the color tuning ability of $Na_5Gd(WO_4)_4$:Tb/Yb, which induces the shift of emission color from yellow-green to green as the temperature increases (Fig. 16a). The obtained maximum sensitivity is 1.3% K^{-1}.[160] In the same year, Li *et al.* achieved a real-time naked-eye recognizable color change based on Ho^{3+}(or Tm^{3+})-activated $NaYF_4$ UC nanowires (Fig. 16b–d), depending on the different spectral sensitivities of the blue, green, and red UC emissions to temperature. The corresponding relative sensitivity of this color change-based thermometer reaches up to 1.83% K^{-1}.[161]

Although the feasibility of color change-based thermometry is demonstrated, the sensitivities are still relatively low, mainly due to the lower performance of these temperature-induced color tuning phenomena.

In 2022, a striking color change with temperature was achieved in heavily doped $LiErF_4$@$LiYF_4$ C–S NCs, indicating the great potentials of this material in non-contact nanothermometry.[67] As shown in Fig. 16c, the ratio of UC intensity determined by the red to green emission increased from 0.62 to 71.54 as the temperature rose. The relative thermal sensitivity can reach as high as 5.27% K^{-1}, which is much higher than that of the thermally-coupled thermometers (typically less than 1.30% K^{-1}) as well as other color change-based thermometers. It is worth noting that the thermally responsive UC showed good stability and reversibility (Fig. 16e), evidencing that this material is ideal for the practical applications.

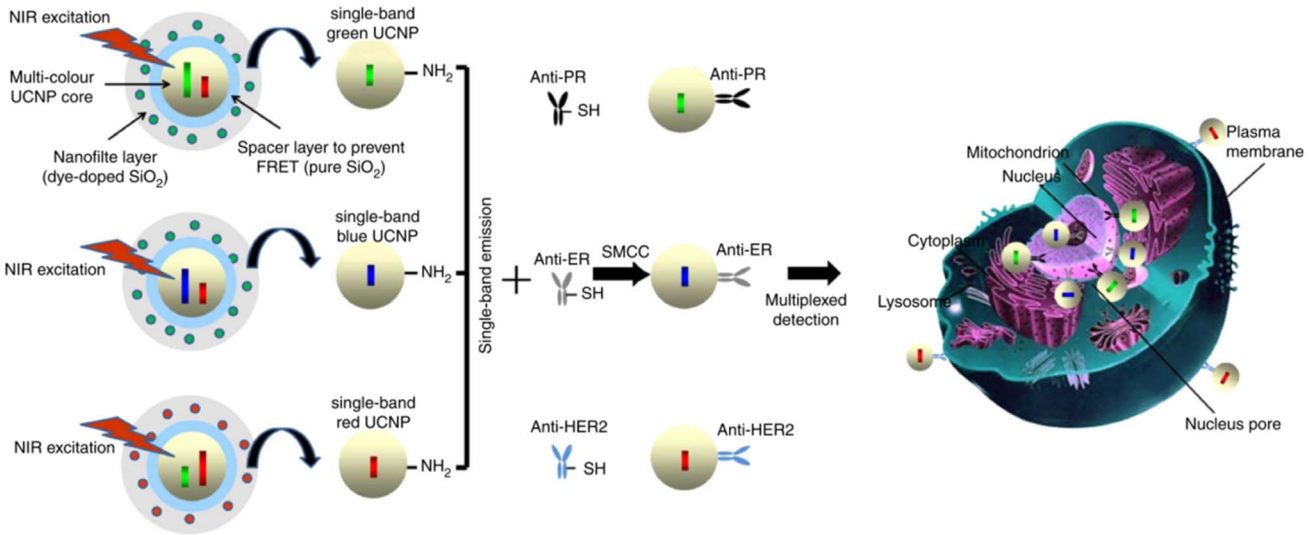

Fig. 17 Schematic diagram of single-band UCNCs fabrication for multiplexed detection. Surface amino modifications formed the R/G/B single-band UCNCs, for multiplexed *in situ* molecular mapping of breast cancer. Reproduced with permission.[171] Copyright 2015, Sprinter Nature.

After that, based on the super-sensitivity temperature response of the Y:75Er@Y C–S NCs, the exponentially enhanced green UC luminescence by more than two orders was obtained under low temperature. Further utilizing the temperature-insensitive blue emission as self-calibration, the formed core–multishell Y:75Er@Y@Y:75Yb/2Tm@Y UCNCs exhibit ultra-high relative sensitivity of 12.3% K^{-1} (Fig. 16f and g).[87] It is noteworthy that although demonstrating the great potential in the field of ultra-sensitive temperature sensing, due to the suppressed phonon-assisted CR processes are the key of this thermometer, it can only achieve high sensitivity under cryonic conditions.

Very recently, researchers reported a design of a C–S–S nanostructure to improve the thermal sensitivity by using the non-thermally coupled UC emissions. Ho^{3+} and Tm^{3+} were selected as emitters and spatially separated by an inert layer. The Tm^{3+} emission showed a dramatic thermal enhancement while the Ho^{3+} showed a decline with increasing temperature, resulting in a large intensity ratio (695 nm/645 nm) contrast and thereafter a high relative sensitivity (9.78% K^{-1}).[162]

4.3 Image-guided bioapplications

Imaging through UCNCs has unique advantages such as no autofluorescence background, high sensitivity, good resolution, deep tissue penetration, high photobleaching resistance, and compatibility with long-term repeated imaging. Especially, the color tuning nature of UCNCs provides additional signal dimensions. They are, therefore, suitable for labeling different targets simultaneously and promising candidate as multifunctional treatment probes.[163–167] In the past decade, color tuning from UCNCs has been utilized successfully in the application fields of multiplexing bioimaging and multimodal therapeutic probe, towards particularly the early-stage diagnosis and targeted treatment of diseases in clinic.

Early-stage multiplexing bioimaging based on multicolor UCNCs involve mostly two colors, green light from Er^{3+} and blue light from Tm^{3+}, due to the lack of pure red emitting UCNCs.

In 2016, multicolor fluorescent probes based on UCNCs labeling and antibody affinity was successfully developed for simultaneous specific sensing of *E. coli* and *S. aureus*. UCNCs with different colors were fabricated *via* varying Ln dopants (blue light from Tm^{3+} and green light from Er^{3+}) to acquire the separated emission peaks to label the corresponding specific bacteria, although the color difference is not significant as the color purities are low.[168] After this, You *et al.* developed a multiplexed UC-Lateral Flow Strip (LFS) platform for HF prognosis at home, which integrated dual-color (green and blue) UCNCs-based LFS and a smartphone-based portable reader.[169]

Till recently, Cheng *et al.* demonstrated successfully the *in vivo* R/G/B multiplexed imaging, based on the re-absorption color tuning mechanism in UCNCs. In this work, the authors developed a facile way, through the absorption of various dyes (Rhodamine B, R6G, and TQ1), to generate R/G/B color of UCNCs for *in vivo* imaging.[170] In 2015, three different antibodies were coupled to multicolor UCNCs to target the three most important breast cancer biomarkers (PR, ER, and HER2), respectively, enabling simultaneous multiplexed *in situ* molecular mapping. As shown in Fig. 17, UCNCs with two emission bands including β-Gd:Yb/Er@Gd with green and red emissions, β-Gd:Yb/Tm@Gd NCs with blue and red emissions, and α-Yb:Er@Y NCs with green and red emissions, were prepared first. Selective nanofilters were then created by coating a silicon layer doped with amino-activated organic dyes outside the NCs, to form the single-band emissions and then the high throughout multiplexing bioimaging.[171]

From another side, the real-time color-tunable UCNCs showed great potentials in targeted treatment of diseases. In 2018, the image-guided photodynamic therapy (PDT) was proposed by Kong *et al.*, utilizing the color-tunable UCNCs@TiO_2. As illustrated in Fig. 18a, under 800 nm laser excitation, only quasi-monochromatic red UC emission is generated for positioning. Once the tumor site is targeted, the excitation switches to 980 nm to induce additional ultraviolet-blue emissions for PDT. Thus, the

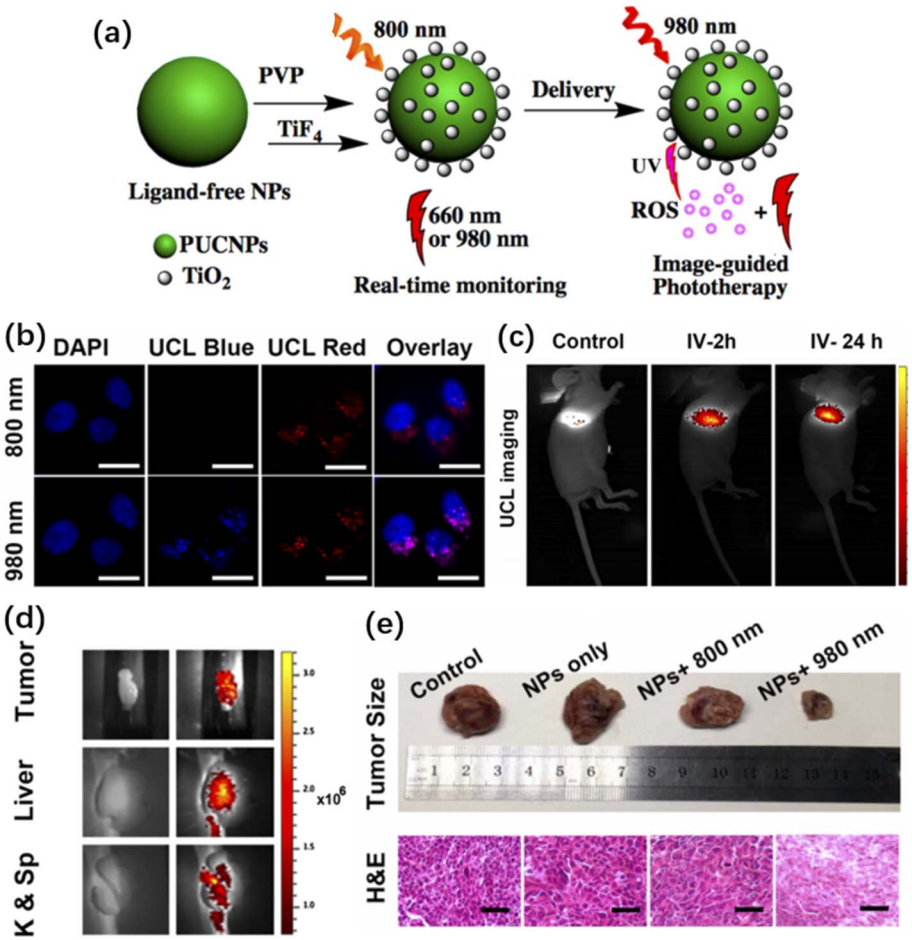

Fig. 18 Multimodal therapeutic probe using color-tunable UCNCs. (a) Scheme of photoswitchable PDT using UCNCs@TiO_2 for real-time monitoring and image-guided phototherapy. (b) A549 cells treated with UCNCs@TiO_2 for imaging with 980 and 800 nm light excitation, respectively, and stained with DAPI. (c) *In vivo* UC imaging of tumor-bearing mouse with UCNCs@TiO_2 under 800 nm laser at 2 and 24 h after intravenous injection. (d) *Ex vivo* UC images of kidney, spleen, liver, and tumor after 24 h post injection, the luminescent intensity of dissected organs further confirmed the preferential accumulation of UCNCs@TiO_2 in tumor and main organs. (e) Photographs to display the excised tumors after various treatment. H&E staining tumor sections harvested from the control group, groups of UCNCs@TiO_2 only and UCNCs@TiO_2 + 800 nm and UCNCs@TiO_2 + 980 nm laser. The scale bars are 50 μm.[118] Copyright 2018, American Chemical Society.

designed color-tunable probes ensure high imaging safety and treatment precision, as demonstrated by the *in vitro*, *in vivo*, and *ex vivo* experiments (Fig. 18b–d), and finally can inhibit the tumor growth significantly (Fig. 18e).[118]

Overall, UCNCs with tunable emission color show great potentials in multiplexing imaging and multimodal treatment. They also have considerable research value in other biological applications like optogenetics, cell biology, and DNA detection. Additionally, combining the temporal dimension of the color-tunable UC can offer significant advantages in optical multiplexing.[166,167]

5. Summary and outlook

In summary, this review mainly described the mechanisms, strategies, results, and applications of color tuning in Ln UCNCs. Firstly, we introduce the mechanisms of photoluminescence and color tuning of Ln UCNCs along with that of the traditional fluorescence dyes and semiconductor QDs. Then, various color tuning strategies and the corresponding examples are summarized. We classify the color tuning of Ln UCNCs into multicolor tuning (*via* inherent properties of NCs) and real-time tuning (*via* external conditions of NCs). Owing to their numerous and unique advantages, color-tunable Ln UCNCs have been perceived as technological marvels that could greatly improve many application fields. Finally, the most promising applications of color-tunable Ln UCNCs are selected and introduced, including fluorescence anti-counterfeiting, temperature sensing, and image-guided bioapplications.

Although significant achievements have been made in the color tuning of Ln UCNCs, challenges and potential opportunities still exist for their wide-spread applications. Thus, we would like to highlight some future directions that may produce pronounced effects in the field:

(i) To introduce new doping compositions available for color tuning. Current UC color tuning uses excitations mostly at

~800 nm (Nd^{3+}), 980 nm (Yb^{3+}), and 1530 nm (Er^{3+}), and the adaptive A^{3+} are mainly Tm^{3+}, Ho^{3+}, and Er^{3+}. Introducing new A^{3+} and S^{3+} into the color tuning family can not only generate more color components but also activate other excitation wavelengths that interact with the NCs, and thus provide more opportunities and means for color tuning. As a precondition, new mechanisms that can release more inactive doping compositions for UC need to be developed.[172] Besides, other non-Ln activators such as the large family of transition metal ions that can cooperate with Ln ions[173] would be considered.

(ii) To prepare ultrasmall color-tunable UCNCs capable of intracellular applications. Small probes are highly useful for the intracellular studies and applications, as sub-10 nm particles can efficiently transport through the subcellular membranes.[174,175] However, for Ln UCNCs the smaller the size means the weaker UC brightness. In addition, color-tunable UCNCs, especially that can be tuned in real-time, usually require multiple-layered C–S structures and tend to be larger particles. Therefore, color-tunable UCNCs with a higher UC efficiency and sub-10 nm size are still needed. Alternatively, the cubic $NaLnF_4$ (α-phase) with much smaller size than its hexagonal counterparts (β-$NaYF_4$) and controllable shell coating (typically cubic CaF_2)[176] deserve deeper investigation towards real-time color tuning within 10 nm scale.

(iii) To develop new host materials prepared *via* facile routes. $NaLnF_4$ NCs are still the most popular host materials for UC color tuning, due to their good stability, low phonon energy, controllable morphology, and feasible C–S structure. But the mostly-used thermal decomposition method for preparing $NaLnF_4$ NCs is complex and time-consuming, especially for their C–S counterparts. Therefore, it is still a major challenge to find a new host material that will maintain stable and bright UC emissions, and meanwhile can be prepared by an easier and faster way than that of $NaLnF_4$ host. Although researchers have developed ultrafast synthesis of new UC hosts with excellent luminescent properties, the limitations like large particle size, poor monodispersity, and difficult to epitaxially grow shells still need to be overcome.[177–179]

(iv) To manipulate the ET with high accuracy. It was previously revealed that the dopants distribute unevenly in the lattice of Ln doped NCs.[180] In addition, the severe penetration of core dopants into the shells was found very recently due to the dynamic of dissolve and growth during the epitaxial growth.[29,128] The uncontrollable distribution of dopants prevents researchers from accurate manipulation of the interactions between neighboring Ln dopants, which is crucial for the UC properties like intensity and color. Elaborate engineering the dopants arrangement *via* more even distribution,[181] suppression of cation exchange,[182] and localized enriching[183] has been proved can greatly improve the UC intensity. As a result, manipulating the ET processes more accurately may be particularly promising for fully releasing the potentials of Ln-based color-tunable UCNCs.

(v) To exploit new applications suitable for color-tunable UCNCs. As described in Section 4 of this review, the current application fields of color-tunable UCNCs are still limited. We believe the wide versatility and high flexibility of color-tunable UCNCs can find more suitable applications. Possible examples can be: individual marking of endangered species[184] owing to the larger dimension of emission color for tunable UCNCs as compared to the widely-used visual implant elastomer (VIE) tags; light color-indicated sensors based on the external condition-induced color tunable materials, like estimation of laser power density using the excitation intensity-induced color tuning; smart wearable devices towards health monitoring *via* pH value-, temperature-, moisture-, and exhalation-induced color change.

(vi) To build up predictable models for UC color tuning. The basic theoretical framework of Ln luminescence was systematically established several decades ago.[185–187] But to date, there is few model that can predict conveniently the UC properties based on the initial parameters of structure and composition of materials, which is especially valuable for color tuning in Ln UCNCs, due to avoiding of time-consuming trial and error and optimization. The lack of predictive modeling can mainly stem from the complicated UC pathways, especially the diverse ET processes. Recently developed machine learning technique have shown great values on prediction of the structure and performance relationship,[188,189] especially for luminescent materials,[190–192] and thus might have an easy way access to customized color-tunable UCNCs.

(vii) Last but not least, to collaborate non-UC and UC luminescence for color tuning. On one hand, other photoluminescence types, such as DS and DC under short-wave excitations like UV light or X-ray, may further expand the toolbox for high-performance color tuning. Consequently, single-band DS and DC emissions with high brightness require more systematical investigation, although there were some good results reported.[193,194] Besides, invisible emissions can be involved in the color tuning, like the solar blind[195] and NIR region,[196] for various application scenarios. Other DS luminescent nanomaterials like CDs and QDs may associate with the color-tunable UCNCs chemically or physically, utilizing their excellent luminescent performance.[197,198] On the other hand, non-photoluminescence processes provide more diverse implementations for the color tuning, and are also promising. For instance, combining perovskite QDs and Ln ions, different emission colors can be generated by applying electric field.[199] Mechanoluminescence materials also exhibits great potential for color tuning as their emission peaks shift when imposition of external force, although the performance of current mechanoluminescence-based color tuning still needs further optimization.[200]

In summary, this review focuses on the color tuning in Ln-doped UCNCs. It analyzes the current research progress in a detailed manner while put forward the challenges and potential opportunities. We believe that Ln-doped UCNCs, which have been highly recognized in various fields such as physics, chemistry, biology, and materials, will fully demonstrate their advantages in color tuning and exhibit their deserved value in the future.

Author contributions

Jiayue Zhang: writing review & investigation. Xinyu Wang: investigation. Yuxin Jin: investigation. Boyang Li: writing review

& investigation. Lu Liu: writing review & editing. Jianzhong Zhang: editing & supervision.

Conflicts of interest

The authors declare that they have no known competing financial interests or personal relationships that could have appeared to influence the work reported in this paper.

Data availability

No primary research results, software or code have been included and no new data were generated or analysed as part of this review.

Acknowledgements

Financial support from the Fundamental Research Funds for the Central Universities (Grant No. 3072024LJ2503).

References

1 M. Y. Zhu, Z. H. Li, X. C. Li, X. C. Li, X. R. Zhang, Y. X. Wang, H. Y. Hao and L. Li, *Sci. Rep.*, 2024, **14**, 7099.
2 P. A. Demakov, A. A. Vasileva, S. S. Volynkin, A. A. Ryadun, D. G. Samsonenko, V. P. Fedin and D. N. Dybtsev, *Molecules*, 2021, **26**, 5145.
3 W. X. Li, J. Hagen, R. Jones, J. Heikenfeld and A. J. Steckl, *Solid-State Electron.*, 2007, **51**, 500.
4 A. Perulli, A. Balena, G. Nedelcu, A. Cretí, M. V. Kovalenko, M. Lomascolo, M. Fernandezd and M. Anni, *Appl. Phys. Lett.*, 2018, **112**, 171904.
5 L. He, Y. W. Zhang, G. L. Ma, P. Tan, Z. J. Li, S. B. Zang, X. Wu, J. Jing, S. H. Fang, L. J. Zhou, Y. J. Wang, Y. Huang, P. G. Hogan, G. Han and Y. B. Zhou, *eLife*, 2015, **4**, e10024.
6 Y. Zhu, L. Xu, B. Y. Li, Y. F. Wang, D. Y. Li, J. Ren, H. L. Jiang, L. Liu, F. G. Jiang and J. Z. Zhang, *Opt. Lett.*, 2022, **47**, 4834.
7 F. Wang and X. G. Liu, *Acc. Chem. Res.*, 2014, **47**, 1378.
8 Z. Zhang, M. K. G. Jayakumar, X. Zheng, S. Shikha, Y. Zhang, A. Bansal, D. J. J. Poon, P. L. Chu, E. L. L. Yeo, M. L. K. Chua, S. K. Chee and Y. Zhang, *Nat. Commun.*, 2019, **10**, 4586.
9 W. B. Wu, M. L. Wang, Y. M. Sun, W. Huang, Y. P. Cui and C. X. Xu, *Opt. Mater.*, 2008, **30**, 1803.
10 C. Ippen, T. Greco, Y. Kim, C. Pries, J. Kim, M. S. Oh, C. J. Han and A. Wedel, *J. Soc. Inf. Disp.*, 2015, **23**, 285.
11 Y. Fu, P. W. Winter, R. Rojas, V. Wang, M. McAuliffe and G. H. Patterson, *Proc. Natl. Acad. Sci. U. S. A.*, 2016, **113**, 4368.
12 J. Yu, X. J. Diao, X. J. Zhang, X. F. Chen, X. J. Hao, W. Li, X. H. Zhang and C. S. Lee, *Small*, 2013, **10**, 1125.
13 L. Hu, H. Z. Wu, Z. F. Wan, C. F. Cai, T. N. Xu, T. G. Lou and B. P. Zhang, *New J. Phys.*, 2012, **14**, 013059.
14 N. Cicek, S. Nizamoglu, T. Ozel, E. Mutlugun, D. U. Karatay, V. Lesnyak and H. V. Demir, *Appl. Phys. Lett.*, 2009, **94**, 061105.
15 M. J. Ortiz, I. Garcia-Moreno, A. R. Agarrabeitia, G. Duran-Sampedro, A. Costela, R. Sastre, F. L. Arbeloa, J. B. Prieto and I. L. Arbeloa, *Phys. Chem. Chem. Phys.*, 2010, **12**, 7804.
16 S. Q. Huang, Z. C. Li, L. Kong, N. W. Zhu, A. D. Shan and L. Li, *J. Am. Chem. Soc.*, 2016, **138**, 5749.
17 X. Y. Xu, R. Ray, Y. L. Gu, H. J. Ploehn, L. Gearheart, K. Raker and W. A. Scrivens, *J. Am. Chem. Soc.*, 2004, **126**, 12736.
18 B. Y. Wang, J. K. Yu, L. Z. Sui, S. J. Zhu, Z. Y. Tang, B. Yang and S. Y. Lu, *Adv. Sci.*, 2021, **8**, 2001453.
19 Y. P. Sun, B. Zhou, Y. Lin, W. Wang, K. A. S. Fernando, P. Pathak, M. J. Meziani, B. A. Harruff, X. Wang, H. F. Wang, P. J. G. Luo, H. Yang, M. E. Kose, B. L. Chen, L. M. Veca and S. Y. Xie, *J. Am. Chem. Soc.*, 2006, **128**, 7756.
20 A. B. Bourlinos, A. Stassinopoulos, D. Anglos, R. Zboril, M. Karakassides and E. P. Giannelis, *Small*, 2008, **4**, 455.
21 Q. L. Zhao, Z. L. Zhang, B. H. Huang, J. Peng, M. Zhang and D. W. Pang, *Chem. Commun.*, 2008, **41**, 5116.
22 X. Miao, D. Qu, D. X. Yang, B. Nie, Y. K. Zhao, H. Y. Fan and Z. C. Sun, *Adv. Mater.*, 2018, **30**, 1704740.
23 L. Ai, Y. S. Yang, B. Y. Wang, J. B. Chang, Z. Y. Tang, B. Yang and S. Y. Lu, *Sci. Bull.*, 2021, **66**, 839.
24 J. C. Boyer, C. J. Carling, B. D. Gates and N. R. Branda, *J. Am. Chem. Soc.*, 2010, **132**, 15766.
25 W. Li, Z. W. Chen, L. Zhou, Z. H. Li, J. S. Ren and X. G. Qu, *J. Am. Chem. Soc.*, 2015, **137**, 8199.
26 X. Chen, L. M. Jin, W. Kong, T. Y. Sun, W. F. Zhang, X. H. Liu, J. Fan, S. F. Yu and F. Wang, *Nat. Commun.*, 2016, **7**, 10304.
27 N. Dubey and S. Chandra, *J. Rare Earths*, 2022, **40**, 1343.
28 T. Chen, Y. F. Shang, S. W. Hao, C. Q. Zhu, Z. T. Lei, X. Wang, W. Q. Lv and C. H. Yang, *Chem. Eng. J.*, 2022, **430**, 131242.
29 A. R. Hong, J. H. Kyhm, G. Kang and H. S. Jang, *Nano Lett.*, 2021, **21**, 4838.
30 X. Liu, H. M. Chen, Y. T. Wang, Y. G. Si, H. X. Zhang, X. M. Li, Z. C. Zhang, B. A. Yan, S. Jiang, F. Wang, S. J. Weng, W. D. Xu, D. Y. Zhao, J. Y. Zhang and F. Zhang, *Nat. Commun.*, 2021, **12**, 5662.
31 M. Wu, L. Yan, T. Wang, B. Zhou and Q. Y. Zhang, *Adv. Funct. Mater.*, 2019, **29**, 1804160.
32 Y. Q. Lu, J. B. Zhao, R. Zhang, Y. J. Liu, D. M. Liu, E. M. Goldys, X. S. Yang, P. Xi, A. Sunna, J. Lu, Y. Shi, R. C. Leif, Y. J. Huo, J. Shen, J. A. Piper, J. P. Robinson and D. Y. Jin, *Nat. Photonics*, 2014, **8**, 32.
33 Y. D. Han, H. Y. Li, Y. B. Wang, Y. Pan, L. Huang, F. Song and W. Huang, *Sci. Rep.*, 2017, **7**, 1320.
34 F. Fan, S. Turkdogan, Z. C. Liu, D. Shelhammer and C. Z. Ning, *Nat. Nanotechnol.*, 2015, **10**, 796.
35 R. R. Deng, F. Qin, R. F. Chen, W. Huang, M. H. Hong and X. G. Liu, *Nat. Nanotechnol.*, 2015, **10**, 237.
36 J. S. Huang, L. Yan, Z. C. An, H. P. Wei, C. Wang, Q. Y. Zhang and B. Zhou, *Adv. Mater.*, 2024, **36**, 2310524.
37 A. Dwivedi, M. Srivastava, A. Dwivedi, A. Srivastava, A. Mishra and S. K. Srivastava, *J. Rare Earths*, 2022, **40**, 8.
38 C. X. Luo, Y. Jing, Z. H. Hua, Z. X. Sui, C. Wang, P. Hu, L. R. Zheng, S. Qian, L. Y. Yang, X. Y. Sun, G. Tang,

H. Cai, Y. Zhu, H. Y. Ban, J. F. Han, Z. L. Wang, X. S. Qiao, J. Ren and J. Z. Zhang, *ACS Appl. Mater. Interfaces*, 2023, **15**, 46266.
39 L. N. Xu, H. Y. Zheng, T. Pang and J. W. Mao, *J. Rare Earths*, 2022, **40**, 406.
40 B. Q. Shao, J. S. Huo and H. P. You, *Adv. Opt. Mater.*, 2019, **7**, 1900319.
41 D. W. Liu, X. X. Xu, Y. Du, X. Qin, Y. H. Zhang, C. S. Ma, S. H. Wen, W. Ren, E. M. Goldys, J. A. Piper, S. X. Dou, X. G. Liu and D. Y. Jin, *Nat. Commun.*, 2016, **7**, 10254.
42 Y. H. Zhang, L. Huang and X. G. Liu, *Angew. Chem., Int. Ed. Engl.*, 2016, **55**, 5718.
43 M. Pan, W. M. Liao, S. Y. Yin, S. S. Sun and C. Y. Su, *Chem. Rev.*, 2018, **118**, 8889.
44 Y. H. Zhang, L. X. Zhang, R. R. Deng, J. Tian, Y. Zong, D. Y. Jin and X. G. Liu, *J. Am. Chem. Soc.*, 2014, **136**, 4893.
45 C. Lu, E. Joulin, H. Tang, H. Pouri and J. Zhang, *Int. J. Mol. Sci.*, 2022, **23**, 9003.
46 S. B. Liu, L. Yan, J. S. Huang, Q. Y. Zhang and B. Zhou, *Chem. Soc. Rev.*, 2022, **51**, 1729.
47 R. T. Wegh, H. Donker, K. D. Oskam and A. Meijerink, *Science*, 1999, **283**, 663.
48 N. Kodama and Y. Watanabe, *Appl. Phys. Lett.*, 2004, **84**, 4141.
49 J. Q. Li, J. S. Liao, H. R. Wen, L. Y. Kong, M. H. Wang and J. L. Chen, *J. Lumin.*, 2019, **213**, 356.
50 K. Binnemans, *Chem. Rev.*, 2009, **109**, 4283.
51 N. Bloembergen, *Phys. Rev. Lett.*, 1959, **2**, 84.
52 F. Auzel, *Chem. Rev.*, 2004, **104**, 139.
53 F. Auzel, *C. R. Acad. Sci.*, 1966, **262**, 1016.
54 F. Auzel, *C. R. Acad. Sci.*, 1966, **263**, 819.
55 C. Lee, E. Z. Xu, Y. W. Liu, A. Teitelboim, K. Y. Yao, A. Fernandez-Bravo, A. M. Kotulska, S. H. Nam, Y. D. Suh, A. Bednarkiewicz, B. E. Cohen, E. M. Chan and P. J. Schuck, *Nature*, 2021, **589**, 230.
56 C. Li, X. Y. Li and X. W. Liu, *ACS Appl. Mater. Interfaces*, 2020, **14**, 10947.
57 M. Pollnau, D. R. Gamelin, S. R. Lűthi and H. U. Gűdel, *Phys. Rev. B:Condens. Matter Mater. Phys.*, 2000, **61**, 3337.
58 F. Wang and X. G. Liu, *J. Am. Chem. Soc.*, 2008, **130**, 5642.
59 C. H. Dong, J. Pichaandi, T. Regier and F. C. J. M. van Veggel, *Nanoscale*, 2011, **3**, 3376.
60 Z. Q. Li, Y. Zhang and S. Jiang, *Adv. Mater.*, 2008, **20**, 4765.
61 X. Y. Xie, Q. Q. Li, H. R. Chen, W. Wang, F. X. Wu, L. P. Tu, Y. L. Zhang, X. G. Kong and Y. L. Chang, *Nano Lett.*, 2022, **22**, 5339.
62 B. Chen and F. Wang, *Nanoscale*, 2018, **10**, 19898.
63 S. Y. Tan, P. P. Yang, N. Niu, S. L. Gai, J. Wang, X. Y. Jing and J. Lin, *J. Alloys Compd.*, 2010, **490**, 684.
64 J. Xie, Z. L. Zhou, S. H. Ma, X. Luo, J. J. Liu, S. Y. Wang, Y. Q. Chen, J. J. H. Yan and F. H. Luo, *Nanoscale Res. Lett.*, 2021, **16**, 131.
65 S. Y. Han, X. Qin, Z. F. An, Y. H. Zhu, L. L. Liang, Y. Han, W. Huang and X. G. Liu, *Nat. Commun.*, 2016, **7**, 13059.
66 H. G. Wen, H. Zhu, X. Chen, T. F. Hung, B. L. Wang, G. Y. Zhu, S. F. Yu and F. Wang, *Angew. Chem., Int. Ed.*, 2013, **52**, 13419.
67 L. Yan, J. S. Huang, Z. An, Q. Y. Zhang and B. Zhou, *Nano Lett.*, 2022, **22**, 7042.
68 Y. Mu, N. Wang, Z. C. Sun, J. Wang, J. Y. Li and J. H. Yu, *Chem. Sci.*, 2016, **7**, 3564.
69 H. Shao, X. Bai, G. C. Pan, H. N. Cui, J. Y. Zhu, Y. Zhai, J. S. Liu, B. Dong, L. Xu and H. W. Song, *Nanotechnology*, 2018, **29**, 285706.
70 P. Chen, H. Jia, Z. Zhong, J. Han, Q. Guo, J. Zhou, X. Liu and J. Qiu, *J. Mater. Chem. C*, 2015, **3**, 8794.
71 S. K. Singh, K. Kumar, M. K. Srivastava, D. K. Rai and S. B. Rai, *Opt. Lett.*, 2010, **35**, 1575.
72 Z. Q. Huo, H. Jia, S. H. Guo, X. R. Feng, J. Zhao, W. X. Liu, L. Yang, W. Y. He, Y. L. Zhang and Y. Y. Teng, *J. Lumin.*, 2024, **273**, 120670.
73 Y. H. Liu, Y. Xue, R. H. Liu, M. Y. Chen, G. T. Chen, C. P. Yan, X. Zhang, Y. N. Zhou, W. Gao and X. L. Ma, *J. Rare Earths*, 2019, **37**, 350.
74 K. Suresh, A. Bankapur, S. Chidangil, H. Madhyastha, K. Sakai and S. D. George, *J. Mater. Chem. C*, 2021, **9**, 8606.
75 D. Q. Chen, M. Xu, P. Huang, M. F. Ma, M. Y. Ding and L. Lei, *J. Mater. Chem. C*, 2017, **5**, 5434.
76 Z. Yin, D. L. Zhou, W. Xu, S. B. Cui, X. Chen, H. Wang, S. H. Xu and H. W. Song, *ACS Appl. Mater. Interfaces*, 2016, **8**, 11667.
77 Z. D. Lei, X. Ling, Q. S. Mei, S. Fu, J. Zhang and Y. Zhang, *Adv. Mater.*, 2020, **32**, 1906225.
78 X. M. Yin, H. Wang, Y. Tian, M. M. Xing, Y. Fu and X. X. Luo, *Nanoscale*, 2018, **10**, 9673.
79 O. Ehlert, R. Thomann, M. Darbandi and T. Nann, *ACS Nano*, 2008, **2**, 120.
80 H. Dong, L. D. Sun, Y. F. Wang, *et al.*, *J. Am. Chem. Soc.*, 2015, **137**(20), 6569–6576.
81 Z. Zhou, D. Ning, Y. Zhu, L. Xu, Y. Yang, E. Zhao, L. Liu and S. Liu, *AIP Adv.*, 2021, **11**, 105312.
82 C. H. Dong and F. C. J. M. van Veggel, *ACS Nano*, 2009, **3**, 123.
83 J. Zhang, C. Cao, J. S. Wang, S. W. Li and Y. Xie, *ACS Appl. Nano Mater.*, 2022, **5**, 16642.
84 H. Jia, N. Li, H. Y. He, X. C. Zhang, Y. Y. Teng and W. P. Qin, *Adv. Opt. Mater.*, 2024, **12**, 2302583.
85 H. Jia, J. Zhao, Z. Q. Huo, X. R. Feng, W. X. Liu, S. H. Guo, N. Li, D. G. Li, Y. Yang, W. Y. He, Y. Y. Teng and W. P. Qin, *Chem. Eng. J.*, 2024, **488**, 150790.
86 V. Lojpur, G. Nikolic and M. D. Dramicanin, *J. Appl. Phys.*, 2014, **115**, 203106.
87 K. F. Wu, E. H. Wang, J. Yuan, J. Zuo, D. Zhou, H. F. Zhao, Y. S. Luo, L. G. Zhang, B. Li, J. H. Zhang, L. P. Tu and H. Zhang, *Angew. Chem., Int. Ed.*, 2023, **62**, e202306585.
88 J. Riegler, O. Ehlert and T. Nann, *Anal. Bioanal. Chem.*, 2006, **384**, 645.
89 J. Riegler and T. Nann, *Anal. Bioanal. Chem.*, 2004, **379**, 913.
90 M. L. Tan, F. Li, X. Wang, R. W. Fan and G. Y. Chen, *ACS Nano*, 2020, **6**, 6532.
91 Y. P. Peng, W. Lu, P. P. Ren, Y. Q. Ni, Y. F. Wang, P. G. Yan, Y. J. Zeng, W. F. Zhang and S. C. Ruan, *Nanomaterials*, 2018, **8**, 497.

92 Z. L. Ji, Y. Cheng, X. S. Cui, H. Lin, J. Xu and Y. S. Wang, *Inorg. Chem. Front.*, 2019, **6**, 110.
93 X. Yang, Z. Y. Wu, Z. N. Yang, X. F. Zhao, C. Q. Song, M. H. Yuan, K. Han, H. Y. Wang, S. Q. Li and X. J. Xu, *J. Alloys Compd.*, 2020, **854**, 157078.
94 M. Ichikawa, Y. Ishikawa, T. Wakasugi and K. Kadono, *Phys. Status Solidi A Appl. Res.*, 2011, **208**, 2809.
95 X. W. Cheng, Y. Pan, Z. Yuan, X. W. Wang, W. H. Su, L. S. Yin, X. J. Xie and L. Huang, *Adv. Funct. Mater.*, 2018, **28**, 1800208.
96 L. Liu, L. K. Lu, L. Xu, D. Y. Tang, C. Liu, M. K. Shahzad, D. Yan, F. Khan, E. M. Zhao and H. Y. Li, *Opt. Lett.*, 2019, **44**, 711.
97 W. Wang, Z. Feng, B. Li, Y. L. Chang, X. Li, X. Yan, R. Z. Chen, X. M. Yu, H. Y. Zhao, G. Y. Lu, X. G. Kong, J. Qian and X. M. Liu, *J. Mol. Cell Biol.*, 2021, **9**, 2899.
98 G. Blasse and B. C. Grabmaier, *Luminescent Materials*, Springer, 1994.
99 J. F. Suyver, J. Grimm, K. W. Krmer and H. U. Güdel, *J. Lumin.*, 2005, **114**, 53.
100 V. M. Igba, M. A. G. Lobato, C. E. R. Garica, A. G. Santibanez, J. O. Uc, E. Hernandez and E. Viesca-Villanueva, *MRS Adv.*, 2024, **30**, 1392.
101 G. S. He, P. P. Markowicz, T. C. Lin and P. N. Prasad, *Nature*, 2002, **415**, 767.
102 J. Wang, F. Wang, C. Wang, Z. Liu and X. G. Liu, *Angew. Chem., Int. Ed.*, 2011, **50**, 10369.
103 J. Z. Huang, J. Q. Li, X. F. Zhang, *et al.*, *Nano Lett.*, 2020, **20**(7), 5236–5242.
104 H. H. Fu, P. F. Peng, R. F. Li, *et al.*, *Nanoscale*, 2018, **10**(19), 9353–9359.
105 B. Chen, W. Kong, N. Wang, G. Y. Zhu and F. Wang, *Chem. Mater.*, 2019, **31**, 4779.
106 Y. N. Huang, Q. B. Xiao, H. S. Hu, *et al.*, *Small*, 2016, **12**(31), 4200–4210.
107 J. B. Zhao, Z. D. Lu, Y. D. Yin, C. Mcrae, J. A. Piper, J. M. Dawes, D. Y. Jin and E. M. Goldys, *Nanoscale*, 2013, **5**, 944.
108 J. Wang, H. W. Song, W. Xu, B. A. Dong, S. Xu, B. T. Chen, W. Yu and S. Zhang, *Nanoscale*, 2013, **5**, 3412.
109 L. Xu, J. M. Zhang, D. H. Gao, K. L. Lu, I. U. Din, M. K. Shahzad, X. Y. Zhang, X. Zhang, H. Z. Chen and E. M. Zhao, *Nanotechnology*, 2019, **30**, 435703.
110 L. P. Tu, K. F. Wu, Y. S. Luo, E. H. Wang, J. Yuan, J. Zuo, D. Zhou, B. Li, J. J. Zhou, D. Y. Jin and H. Zhang, *Angew. Chem., Int. Ed.*, 2023, **62**, e202217100.
111 F. Vetrone, R. Naccache, V. Mahalingam, C. G. Morgan and J. A. Capobianco, *Adv. Funct. Mater.*, 2009, **19**, 2924.
112 F. Wu, X. M. Liu, X. G. Kong, Y. L. Zhang, L. P. Tu, K. Liu, S. G. Song and H. Zhang, *Appl. Phys. Lett.*, 2013, **102**, 243104.
113 X. Y. Huang and J. Lin, *J. Mater. Chem. C*, 2015, **3**, 7652.
114 D. M. Yang, C. X. Li, G. G. Li, M. M. Shang, X. J. Kang and J. Lin, *J. Mater. Chem.*, 2011, **21**, 5923.
115 M. Guan, M. S. Molokeev and J. J. Zhou, *J. Lumin.*, 2020, **224**, 117289.
116 X. M. Li, Z. Z. Guo, T. C. Zhao, Y. Lu, L. Zhou, D. Y. Zhao and F. Zhang, *Angew. Chem., Int. Ed.*, 2016, **55**, 2464.
117 H. Dong, L. D. Sun, W. Feng, Y. Y. Gu, F. Y. Li and C. H. Yan, *ACS Nano*, 2017, **11**, 3289.
118 J. Zuo, L. P. Tu, Q. Q. Li, Y. S. Feng, I. Que, Y. L. Zhang, X. M. Liu, B. Xue, L. J. Cruz, Y. L. Chang, H. Zhang and X. G. Kong, *ACS Nano*, 2018, **12**, 3217.
119 H. L. Wen, H. Zhu, X. Chen, T. F. Hung, B. L. Wang, G. Y. Zhu, S. F. Yu and F. Wang, *Angew. Chem., Int. Ed.*, 2013, **52**, 13419.
120 L. Liu, D. Yan, L. Xu, Z. W. Zhou, X. H. Sun, Y. Liu, X. Y. Zong, E. M. Zhao, J. Ren, J. Z. Zhang and H. Y. Li, *J. Lumin.*, 2020, **224**, 117306.
121 J. P. Lai, Y. X. Zhang, N. Pasquale and K. B. Lee, *Angew. Chem., Int. Ed.*, 2014, **53**, 14419.
122 L. Wang, H. Dong, Y. N. Li, R. Liu, Y. F. Wang, H. K. Bisoyi, L. D. Sun, C. H. Yan and Q. Li, *Adv. Mater.*, 2015, **27**, 2065.
123 J. C. Boyer and F. C. van Veggel, *Nanoscale*, 2010, **2**, 1417.
124 Y. T. Zhong, G. Tian, Z. J. Gu, Y. J. Yang, L. Gu, Y. L. Zhao, Y. Ma and J. N. Yao, *Adv. Mater.*, 2014, **26**, 2831.
125 L. Liu, K. L. Lu, L. Xu, D. Y. Tang, C. Liu, M. K. Shahzad, D. Yan, F. Khan and E. M. Zhao, *Opt. Lett.*, 2019, **44**, 711.
126 Z. W. Zhou, Y. Liu, X. H. Sun, L. Xu, F. Khan, Y. Z. Li, L. Li, H. Y. Li, J. Ren, J. Z. Zhang and L. Liu, *Opt. Lett.*, 2021, **46**, 900.
127 J. F. Sun, D. Yan and L. Liu, *J. Lumin.*, 2020, **41**, 1.
128 K. R. Mun, J. H. Kyhm, J. Y. Lee, S. Shin, Y. Y. Zhu, G. M. Kang, D. Kim, R. R. Deng and H. S. Jang, *Nano Lett.*, 2023, **23**, 3014.
129 D. Avram, A. A. Patrascu, I. Porosnicu and C. Tiseanu, *Opt. Mater. Express*, 2022, **12**, 1894.
130 H. Naruke, T. Mori and T. Yamase, *Opt. Mater.*, 2009, **31**, 1483.
131 H. Y. Li, X. Sun, M. K. Shahzad and L. Liu, *J. Mater. Chem. C*, 2019, **7**, 7984.
132 D. L. Gao, D. P. Tian, G. Q. Xiao, B. Chong, G. H. Yu and Q. Pang, *Opt. Lett.*, 2015, **40**, 3580.
133 D. Wu, T. Pang, Y. Ji, P. Z. Qiu and Z. X. Zhou, *Spectrochim. Acta, Part A*, 2024, **316**, 124318.
134 X. Y. Wang, R. F. Wang, Y. X. Jin, J. T. Liu, Y. S. Chu, Ye. Tian, J. Ren, L. Liu and J. Z. Zhang, *J. Mater. Chem. C*, 2025, **13**, 13890.
135 F. Auzel, *Phys. Rev. B:Condens. Matter Mater. Phys.*, 1976, **13**, 2809.
136 R. Wang, X. L. Zhang, F. Liu, Y. J. Chen and L. Liu, *Opt. Mater.*, 2015, **43**, 18.
137 S. F. Liu, H. Ming, J. Cui, S. B. Liu, W. X. You, X. Y. Ye, Y. M. Yang, H. P. Nie and R. X. Wang, *J. Phys. Chem. C*, 2018, **122**, 16289.
138 J. J. Leal, E. Rodriguez, C. G. N. Dino, M. C. M. Orozco, F. Gaxiola and R. Narro-Garcia, *Mater. Res. Bull.*, 2021, **144**, 111483.
139 X. F. Wu, S. P. Zhan, J. B. Han and Y. X. Liu, *Nano Lett.*, 2021, **21**, 272.
140 C. D. S. Brites, X. J. Xie, M. L. Debasu, X. Qin, R. F. Chen, W. Huang, J. Rocha, X. G. Liu and L. D. Carlos, *Nat. Nanotechnol.*, 2016, **11**, 851.

141 C. Zhang, L. Yang, J. Zhao, B. H. Liu, M. Y. Han and Z. P. Zhang, *Angew. Chem., Int. Ed.*, 2015, **54**, 11531.
142 M. Hu, D. D. Ma, C. C. Liu, J. Wang, Z. X. Zhang and L. J. Meng, *J. Mater. Chem. C*, 2016, **4**, 6975.
143 M. Sakai, T. Seki and Y. Takeoka, *Small*, 2018, **14**, 1800817.
144 R. A. Janjua, L. Xu, X. Y. Wang, J. J. Carvajal, R. L. Zhang, L. Liu and S. L. He, *Mater. Horiz.*, 2025, DOI: 10.1039/d5mh01409c.
145 L. J. Ding and X. D. Wang, *J. Am. Chem. Soc.*, 2020, **31**, 13558.
146 K. Jiang, L. Zhang, J. F. Lu, C. X. Xu, C. Z. Cai and H. W. Lin, *Angew. Chem., Int. Ed.*, 2016, **128**, 7347.
147 W. Zheng, P. Huang, Z. L. Gong, D. T. Tu, J. Xu, Q. L. Zou, R. F. Li, W. W. You, J. C. G. Bünzli and X. Y. Chen, *Nat. Commun.*, 2018, **9**, 3462.
148 L. Lei, X. R. Dai, Y. Cheng, Y. S. Wang, Z. Xiao and S. Q. Xu, *J. Mater. Chem. C*, 2019, **7**, 3342.
149 J. M. Meruga, W. M. Cross, P. S. May, Q. A. Luu, G. A. Crawford and J. J. Kellar, *Nanotechnology*, 2012, **23**, 395201.
150 M. L. You, M. Lin, S. R. Wang, X. M. Wang, G. Zhang, Y. Hong, Y. Q. Dong, G. R. Jin and F. Xu, *Nanoscale*, 2016, **8**, 10096.
151 L. Liu, D. Yan, L. Xu, Z. W. Zhou, X. H. Sun, Y. Liu, X. Y. Zong, E. M. Zhao, J. Ren, J. Z. Zhang and H. Y. Li, *J. Lumin.*, 2020, **224**, 117306.
152 Q. Y. Shao, G. T. Zhang, L. L. Ouyang, Y. Q. Hu, Y. Dong and J. Q. Jiang, *Nanoscale*, 2017, **9**, 12132.
153 X. W. Liu, Y. Wang, X. Y. Li, Z. G. Yi, R. R. Deng, L. L. Liang, X. J. Xie, D. T. B. Loong, S. Y. Song, D. Y. Fan, A. H. All, H. J. Zhang, L. Huang and X. G. Liu, *Nat. Commun.*, 2017, **8**, 899.
154 X. C. Qiu, Q. W. Zhou, X. J. Zhu, Z. G. Wu, W. Feng and F. Y. Li, *Nat. Commun.*, 2020, **11**, 4.
155 X. J. Zhu, W. Feng, J. Chang, Y. W. Tan, J. C. Li, M. Chen, Y. Sun and F. Y. Li, *Nat. Commun.*, 2016, **7**, 10437.
156 V. Kesarwani and V. K. Rai, *Methods Appl. Fluoresc.*, 2022, **10**, 034006.
157 S. A. Wade, S. F. Collins and G. W. Baxter, *J. Appl. Phys.*, 2003, **94**, 4743.
158 L. X. Peng, Y. Zhou, F. Qin, L. P. Li and Z. G. Zhang, *Opt. Lett.*, 2021, **46**, 9592.
159 D. Jaque and F. Vetrone, *Nanoscale*, 2012, **4**, 4301.
160 G. Xue, X. Chen, C. X. Zheng, G. Q. Wang and L. Y. Li, *Chin. J. Struct. Chem.*, 2020, **39**, 301.
161 D. D. Li, W. Y. Lai, X. Q. Shen, Q. Y. Shao and W. Huang, *Mater. Chem. Front.*, 2019, **3**, 791.
162 H. Z. Huang, H. Tuxun, K. X. Zhong, J. S. Huang, H. P. Wei and B. Zhou, *ACS Appl. Nano Mater.*, 2024, **7**, 7794.
163 Y. Shen, J. H. Zhou, T. R. Liu, Y. T. Tao, R. B. Jiang, M. X. Liu, G. H. Xiao, J. H. Zhu, Z. K. Zhou, X. H. Wang, C. J. Jin and J. F. Wang, *Nat. Commun.*, 2013, **4**, 2381.
164 B. Z. Tian, T. Cohen-Karni, Q. Qing, X. J. Duan, P. Xie and C. M. Lieber, *Science*, 2010, **329**, 830.
165 G. S. Hong, A. L. Antaris and H. J. Dai, *Nat. Biomed. Eng.*, 2017, **1**, 0010.
166 D. H. Ortgies, M. Tan, E. C. Ximendes, R. B. Del, J. Hu, L. Xu, X. D. Wang, E. M. Rodriguez, C. Jacinto and N. Fernandez, *ACS Nano*, 2018, **12**, 4362.
167 G. X. Yang, D. Yang, P. P. Yang, R. C. Lv, C. X. Li, C. N. Zhong, F. He, S. L. Gai and J. Lin, *Chem. Mater.*, 2015, **27**, 7957.
168 B. Zhang, H. H. Li, W. X. Pan, Q. S. Chen, Q. Ouyang and J. W. Zhao, *Food Anal. Methods*, 2017, **10**, 2036.
169 M. L. You, M. Lin, Y. Gong, S. R. Wang, A. Li, L. Y. Ji, H. X. Zhao, K. Ling, T. Wen, Y. Huang, D. F. Gao, Q. Ma, T. Z. Wang, A. Q. Ma, X. L. Li and F. Xu, *ACS Nano*, 2017, **11**, 6261.
170 L. A. Cheng, K. Yang, M. W. Shao, S. T. Lee and Z. A. Liu, *J. Phys. Chem. C*, 2011, **115**, 2686.
171 L. Zhou, R. Wang, C. Yao, X. M. Li, C. L. Wang, X. Y. Zhang, C. J. Xu, A. J. Zeng, D. Y. Zhao and F. Zhang, *Nat. Commun.*, 2015, **6**, 7350.
172 L. Xu, Y. Liu, Z. Zhou, X. Sun, I. U. Din, F. Khan, Y. Li, H. Li, J. Ren, J. J. Carvajal, J. Zhang and L. Liu, *Nanoscale*, 2021, **13**, 9978.
173 X. Y. Li, X. W. Liu, D. M. Chevrier, X. Qin, X. J. Xie, S. Y. Song, H. J. Zhang, P. Zhang and X. G. Liu, *Angew. Chem., Int. Ed.*, 2015, **54**, 13312.
174 A. Gnach, T. Lipinski, A. Bednarkiewicz, J. Rybka and J. A. Capobianco, *Chem. Soc. Rev.*, 2015, **44**, 1561.
175 F. Zhang, *Photon Upconversion Nanomaterials*, Springer, 2015, p. 416.
176 C. Cao, G. S. Li, Y. Xie, C. Hong and Y. Li, *Inorg. Chem. Commun.*, 2021, **126**, 108468.
177 P. P. Lei, R. An, S. Yao, Q. S. Wang, L. L. Dong, X. Xu, K. M. Du, J. Feng and H. J. Zhang, *Adv. Mater.*, 2017, **29**, 1700505.
178 X. L. Gao, F. Song, D. D. Ju, A. H. Zhou, A. N. Khan, Z. Y. Chen, X. Sang, M. Feng and L. S. Liu, *CrystEngComm*, 2020, **22**, 7066.
179 P. P. Lei, Y. Liang, P. Y. Du, Y. Zhang and H. J. Zhang, *CCS Chem.*, 2024, **6**, 1512–1522.
180 X. X. Xu, C. Clarke, C. S. Ma, M. Das, M. Guan, D. M. Liu, L. Wang, A. Tadich, Y. Du, C. Ton-That and D. Y. Jin, *Nanoscale*, 2017, **9**, 7719.
181 X. M. Li, R. Wang, F. Zhang and D. Y. Zhao, *Nano Lett.*, 2014, **14**, 3634.
182 J. Wang, S. S. Zheng, H. J. Zhang, Y. H. Wu, J. Zhang, J. L. Liu, X. H. Zhu and Y. Zhang, *ACS Appl. Nano Mater.*, 2023, **6**, 6398.
183 B. Zhou, B. Tang, C. Zhang, C. Y. Qin, Z. J. Gu, Y. Ma, T. Y. Zhai and J. N. Yao, *Nat. Commun.*, 2020, **11**, 1174.
184 A. Jungwirth, V. Balzarini, M. Zöttl, A. Salzmann, M. Taborsky and J. G. Frommen, *Behav. Ecol. Sociobiol.*, 2019, **73**, 49.
185 D. L. Dexter, *J. Chem. Phys.*, 1953, **21**, 836.
186 B. R. Judd, *Phys. Rev.*, 1962, **127**, 750.
187 L. A. Riseberg and H. W. Moos, *Phys. Rev.*, 1968, **174**, 429.
188 M. Wang, T. Wang, P. Q. Cai and X. D. Chen, *Small Methods*, 2019, **3**, 1900025.
189 M. Mousavizadegan, A. Firoozbakhtian, M. Hosseini and H. X. Ju, *Trends Anal. Chem.*, 2023, **167**, 117216.

190 F. Yang, Y. Wang, X. Jiang, B. Lin and R. Lv, *ACS Comb. Sci.*, 2020, **22**, 285.
191 Y. Zhuo, A. M. Tehrani, A. O. Oliynyk, A. C. Duke and J. Brgoch, *Nat. Commun.*, 2018, **9**, 4377.
192 Y. Wei, P. P. Dang, Z. G. Dai, G. G. Li and J. Lin, *Chem. Mater.*, 2021, **33**, 5496.
193 L. Lei, Y. B. Wang, W. X. Xu, R. G. Ye, Y. J. Hua, D. G. Deng, L. Chen, P. N. Prasad and S. Q. Xu, *Nat. Commun.*, 2022, **13**, 5739.
194 D. L. Gao, J. Gao, F. Gao, Q. Q. Kuang, Y. Pan, Y. F. Chen and Z. W. Pan, *J. Mater. Chem. C*, 2021, **9**, 16634.
195 X. L. Wang, Y. F. Chen, F. Liu and Z. W. Pan, *Nat. Commun.*, 2020, **11**, 2040.
196 S. J. Zhang, J. Li, Z. W. Zhou, Y. Zhu, D. Y. Ning, J. Ren, L. Liu and J. Z. Zhang, *Opt. Express*, 2021, **29**, 42974.
197 M. X. Li, W. T. Liu, T. S. Yang, Q. F. Xu, H. F. Mu, J. Han, K. J. Cao, M. M. Jiao, M. L. Liu, S. F. Zhang, X. M. Tan and C. A. L. Yang, *Opt. Express*, 2023, **31**, 2956.
198 W. Lian, D. T. Tu, P. Hu, X. R. Song, Z. L. Gong, T. Chen, J. B. Song, Z. Chen and X. Y. Chen, *Nano Today*, 2020, **35**, 100943.
199 D. L. Zhou, D. L. Liu, G. C. Pan, X. Chen, D. Y. Li, W. Xu, X. Bai and H. H. Song, *Adv. Mater.*, 2017, **29**, 1704149.
200 S. Wu, P. X. Xiong, D. L. Jiang, B. L. Xiao, Y. Xiao, Y. Chen and Y. Z. Wang, *Chem. Eng. J.*, 2023, **469**, 143961.